OPEN ACCESS Freely available online

PLoS one

Time-Lapse Imaging Reveals Symmetric Neurogenic Cell Division of GFAP-Expressing Progenitors for Expansion of Postnatal Dentate Granule Neurons

Takashi Namba[1,2], Hideki Mochizuki[3], Ryusuke Suzuki[4], Masafumi Onodera[5], Masahiro Yamaguchi[6], Hideo Namiki[2], Seiji Shioda[4], Tatsunori Seki[1,7]*

1 Department of Anatomy, Juntendo University School of Medicine, Tokyo, Japan, **2** Integrative Bioscience and Biomedical Engineering, School of Science and Engineering, Waseda University, Tokyo, Japan, **3** Department of Neurology, Kitasato University School of Medicine, Kanagawa, Japan, **4** Department of Anatomy, Showa University School of Medicine, Tokyo, Japan, **5** Department of Hematology, Institute of Clinical Medicine, University of Tsukuba, Ibaraki, Japan, **6** Departments of Otolaryngology and Physiology, Graduate School of Medicine, University of Tokyo, Tokyo, Japan, **7** Department of Histology and Neuroanatomy, Tokyo Medical University, Tokyo, Japan

Abstract

Granule cells in the hippocampus, a region critical for memory and learning, are generated mainly during the early postnatal period but neurogenesis continues in adulthood. Postnatal neuronal production is carried out by primary progenitors that express glial fibrillary acidic protein (GFAP) and they are assumed to function as stem cells. A central question regarding postnatal dentate neurogenesis is how astrocyte-like progenitors produce neurons. To reveal cell division patterns and the process of neuronal differentiation of astrocyte-like neural progenitors, we performed time-lapse imaging in cultured hippocampal slices from early postnatal transgenic mice with mouse GFAP promoter-controlled enhanced green fluorescent protein (mGFAP-eGFP Tg mice) in combination with a retrovirus carrying a red fluorescent protein gene. Our results showed that the majority of GFAP-eGFP+ progenitor cells that express GFAP, Sox2 and nestin divided symmetrically to produce pairs of GFAP+ cells (45%) or pairs of neuron-committed cells (45%), whereas a minority divided asymmetrically to generate GFAP+ cells and neuron-committed cells (10%). The present results suggest that a substantial number of GFAP-expressing progenitors functions as transient amplifying progenitors, at least in an early postnatal dentate gyrus, although a small population appears to be stem cell-like progenitors. From the present data, we discuss possible cell division patterns of adult GFAP+ progenitors.

Citation: Namba T, Mochizuki H, Suzuki R, Onodera M, Yamaguchi M, et al. (2011) Time-Lapse Imaging Reveals Symmetric Neurogenic Cell Division of GFAP-Expressing Progenitors for Expansion of Postnatal Dentate Granule Neurons. PLoS ONE 6(9): e25303. doi:10.1371/journal.pone.0025303

Editor: Cesario V. Borlongan, University of South Florida, United States of America

Received February 26, 2011; **Accepted** August 31, 2011; **Published** September 23, 2011

Funding: This study was supported by a Grant-in-Aid for Scientific Research from the Japan Society for the Promotion of Science (17500238 and 22500306) and in part by a High Technology Research Center Grant from the Japanese Ministry of Education, Culture, Sports, Science and Technology. The funders had no role in study design, data collection and analysis, decision to publish, or preparation of the manuscript.

Competing Interests: The authors have declared that no competing interests exist.

* E-mail: sekit@tokyo-med.ac.jp

Introduction

The granule cells of the hippocampal dentate gyrus are produced mainly during the early postnatal period, and neurogenesis continues throughout life [1,2,3,4]. The neurogenic activity is implicated in physiological conditions, such as learning, enriched environments and stress, and also pathological conditions such as temporal epilepsy, ischemia and mental diseases [4,5,6,7,8,9]. Understanding these physiological and pathological regulatory mechanisms of postnatal neurogenesis requires detailed knowledge of the neurogenic processes of neural progenitor cells.

Interestingly, the persistent neuronal production from early postnatal to adult stages is carried out by astrocyte-like progenitor cells that express glial fibrillary acidic protein (GFAP) [10,11,12]. The course of neurogenesis from astrocyte-like progenitors has been well investigated in the adult hippocampal neurogenic zone and subgranular zone (SGZ), mainly by pulse-chase experiments with BrdU. The primary progenitors (Type 1 or B cells) have astrocytic features that include expression of GFAP in addition to radial morphology and nestin expression [2,10,11,12,13,14,15,16,17]. The primary progenitors are thought to divide slowly and generate the subsequent intermediate progenitor and another primary progenitor. The next intermediate or amplifying progenitor (Type 2–3, or D cells) expressing neuronal markers such as Hu, Neurogenin2, Tbr2, PSA-NCAM and DCX is considered to divide rapidly to produce immature neurons or neuron-committed progenitors [13,18,19,20].

GFAP-expressing neurogenic progenitors are also found in the early postnatal dentate gyrus [2,21], although the early postnatal dentate gyrus has a broader neurogenic region which corresponds to nearly the entire hilus and subgranular zone (SGZ) [1,2]. In the early postnatal neurogenic zones, a majority of proliferating cells are astrocyte-like cells expressing GFAP, GLAST, nestin and S100β, most of which are not typical radial cells, but are round or elongated cells with relatively short processes and which finally differentiate into granule cells [2,21]. A previous study using GFAP-Cre mice demonstrates the origin of postnatally generated neurons to be the GFAP+ progenitor [10]. During the early postnatal period, astrocyte-like proliferating cells fill the entire areas of the early postnatal neurogenic zones, hilus and SGZ

transiently, but with aging the neurogenic zones gradually become restricted to the SGZ [1,2].

Despite these extensive studies, there is no information as to the actual cell division patterns of GFAP+ primary progenitors, which is essential to determine the exact profile of progenitor cells. In the developing neocortex, precise knowledge about the property of progenitors has been acquired by observation of the cell division pattern using a time-lapse imaging system [22,23,24]. In the present study, to reveal the dynamic cell division patterns and neuronal differentiation processes of GFAP+ primary progenitors, we performed time-lapse imaging analysis of hippocampal slices from postnatal days (P) 4–6 in transgenic mice with mouse GFAP promoter-controlled enhanced green fluorescent protein (mGFAP-eGFP Tg mice) [25]. We used postnatal hippocampal slices in the present study for the following reasons: 1) adult slices are generally not suitable for organotypic slice cultures [26], 2) even in the early postnatal period, dentate granule neurons are produced by GFAP+ progenitors [2], and 3) in slice cultures of the early postnatal hippocampus, GFAP progenitors can differentiate into neurons [21,27]. In the present time-lapse imaging analysis, we employed a short-term slice culture system using collagen-coated glass bottom dishes that we developed previously [20], because this system provides sharper images than the commonly used filter culture systems which are typically employed for hippocampal organotypic cultures [28,29,30], and long-term culture in filter culture systems results in a significant reduction of the capacity of neurogenic activity of proliferating progenitor cells [21]. The present time-lapse experiments in this slice culture system revealed that a major symmetric cell division pattern of astrocyte-like progenitors gave rise to neurons through progenitors expressing GFAP and neuronal markers, simultaneously.

Results

Characterization of dividing cells in the neonatal dentate gyrus

To analyze the nature of dividing cells in the early postnatal dentate gyrus, dividing cell pairs in late anaphase and telophase stained with antibodies to Ki67, GFAP and Hu were counted in the hilus and SGZ. All dividing cell pairs symmetrically expressed molecular markers, of which 62.2% were GFAP+, 17.3% were GFAP+/Hu+ and 7.9% were Hu+ (Fig. 1). This suggests that most dividing cells in the early postnatal dentate gyrus expressed GFAP, in agreement with our previous BrdU-labeling experiments, which also demonstrated that GFAP+ proliferating cells are able to differentiate into neurons *in vivo* and *in vitro* [2,21].

Properties and division patterns of eGFP+ proliferating cells

To analyze the fate of GFAP+ dividing cells, we performed time-lapse imaging of cultured hippocampal slices obtained from GFAP-eGFP Tg mice. In this experiment, we focused on dividing eGFP-positive (eGFP+) cells in the SGZ and hilus of the dentate gyrus. In total, the fates of 79 daughter cell pairs were monitored. After culture, the hippocampal slices were fixed, and the fates of the daughter cells were examined by immunohistochemistry. The time at which 1 eGFP+ cell divided into 2 daughter cells was regarded as time zero (0 hours) (Figure S1). The properties of the daughter cells at the end of the culture were analyzed at 4 culture times after cell division, namely, 0 hours (n = 25 pairs), 2–10 hours (n = 24 pairs), 12–20 hours (n = 19 pairs) and 22–28 hours (n = 11 pairs) (Fig. 2A), because the cell cycle durations of postnatal dentate progenitors are estimated to be 12–14 hours [31] or 24.7 hours [32].

At 0 hours, the majority of eGFP+ daughter cell pairs expressed GFAP (88.0%, Fig. 2B) and the progenitor cell marker nestin (Figure S2). Only 12.0% of the cell pairs were positive for both GFAP and Hu. Neither the Hu+ cell pair nor the asymmetric pair was observed at 0 hours. At each time window, the proportion of the number of 2 identical daughter cell pairs among all eGFP+ daughter cell pairs was much higher than that of 2 different daughter cell pairs (0 hours, 100% vs. 0% [25 pairs vs. 0 pairs]; 2–10 hours, 91.7% vs. 8.3% [22 pairs vs. 2 pairs]; 12–20 hours, 84.2% vs. 15.8% [16 pairs vs. 3 pairs]; 22–28 hours, 90.9% vs. 9.1% [10 pairs vs. 1 pair]), suggesting that the principal division mode of GFAP-expressing progenitor cells was symmetric (Fig. 2A).

Fates of symmetrically divided eGFP+ cells

The percentages of the GFAP+ cell pairs and GFAP+/Hu+ cell pairs changed during the culture period. Specifically, the percentage of GFAP+ cell pairs decreased from 88.0% at 0 hours to 45.5% at the end of culture, whereas the percentage of GFAP+/Hu+ daughter cell pairs increased from 12.0% to 45.5% with time

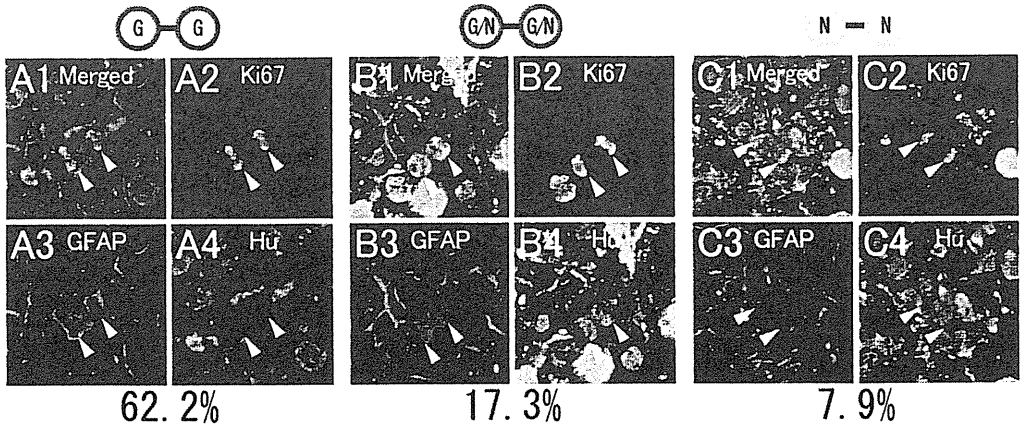

Figure 1. Characterization of dividing cells in the neonatal dentate gyrus. P5 mice were fixed and then processed for immunohistochemistry. The prepared slices were stained with Ki67 (A2, B2, C2), GFAP (A3, B3, C3) and Hu (A4, B4, C4). A: A Ki67+ dividing cell pair expresses GFAP but not Hu. B: A Ki67+ dividing cell pair expresses both GFAP and Hu. C: A Ki67+ dividing cell pair expresses Hu but not GFAP. Scale bar, 10 μm.
doi:10.1371/journal.pone.0025303.g001

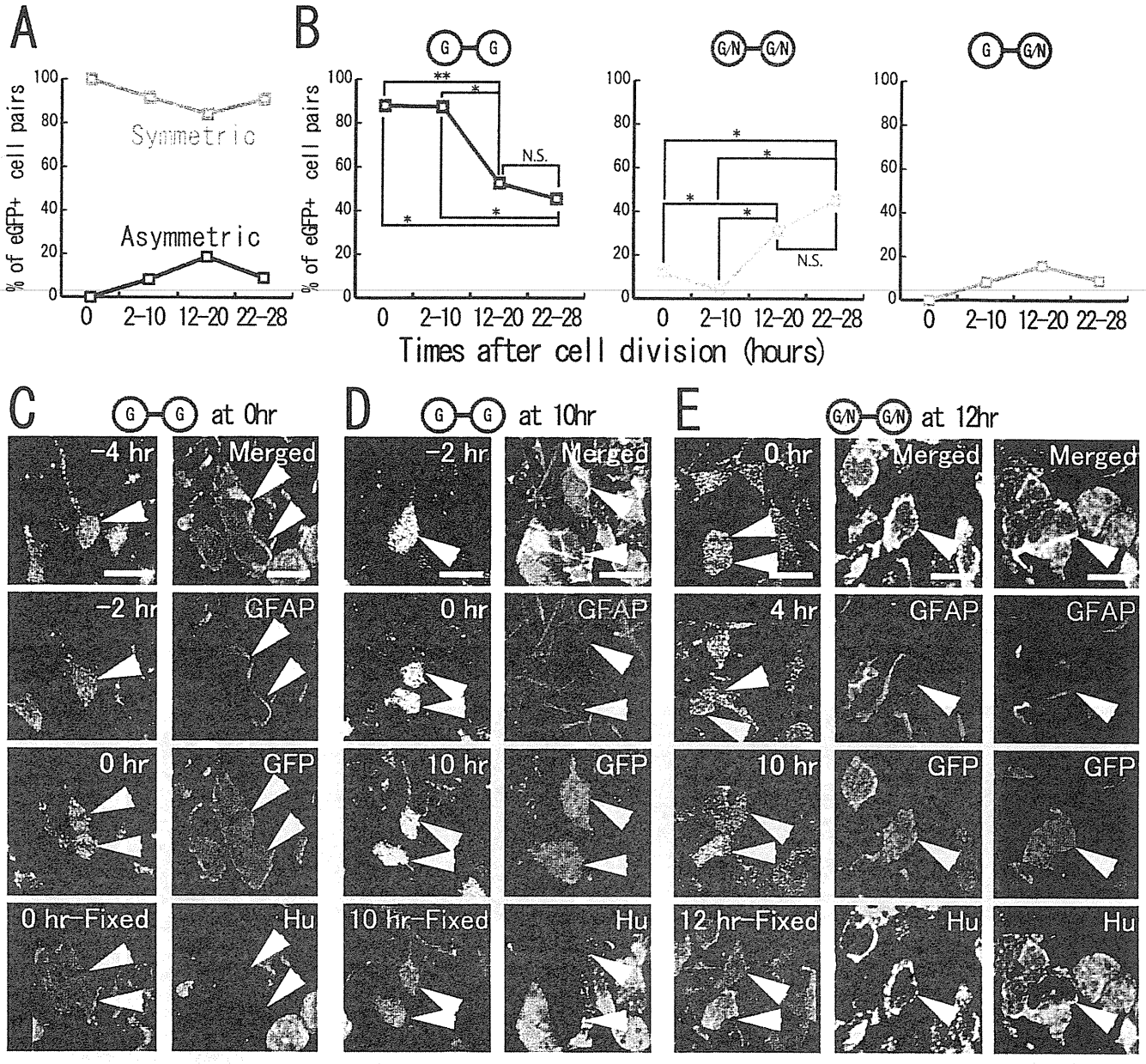

Figure 2. Fates of eGFP+ daughter cells. A: The percentage of eGFP+ cell pairs expressing cell-type specific markers symmetrically or asymmetrically is shown according to the time after cell division. B: The percentage of eGFP+ cell pairs expressing GFAP or Hu is shown according to the time after cell division. C, D, E: Time-lapse imaging of eGFP+ cells (left column) and daughter cell fates at the end of culture (others). E: In the 12-hour fixed section, optical images were projected. Since each cell (arrowheads) was located at a different level of the Z-axis, they are shown separately in the middle and right columns as single z-plane images. Full time-scale images and videos are shown in the supplementary information. G: GFAP+ cells, G/N: GFAP+/Hu+ cells. Scale bar, 10 μm.
doi:10.1371/journal.pone.0025303.g002

after cell division (Fig. 2B, C, D, E; Figs. S2, S3, S4; Videos S1 and S2). This reciprocal change suggests that GFAP+ daughter cells gradually differentiated into GFAP+/Hu+ cells after cell division. To verify the neuronal identity of the GFAP+/Hu+ cells, we attempted to characterize these cells using three different marker antibodies for the neuronal lineage-committed cells, namely, Tbr2, NeuroD and Prox1. These markers can distinguish the different stages of the neuronal lineage-committed cells (Tbr2: early neuronal progenitors; NeuroD: late neuronal progenitors; Prox1: granule cells) [33,34]. In the P5 GFAP-eGFP mouse hippocampus, the eGFP+/GFAP+/Hu+ cells were rarely labeled by NeuroD and Prox1 antibodies. In contrast, 91.1% of the eGFP+/GFAP+/Hu+ cells expressed Tbr2 (a total of 135 cells were counted; Figure S5), suggesting that the GFAP+/Hu+ daughter cells are early-stage neuron-committed cells. Although the GFAP+/Hu+ cells may have finally differentiated into immature neurons, eGFP cells solely expressing neuronal markers, such as Hu or NeuroD, were not detected in the present time-lapse observation, possibly because neuronal differentiation was accompanied by a decrease in GFAP promoter activity resulting in a loss of eGFP.

As 40.9% of the daughter cells lost eGFP fluorescence during the observation period, we could not determine the final fates of these cells. To determine if they finally differentiated into neurons, a retrovirus carrying a red fluorescent protein (HuKO) was

injected into the dentate gyrus of P3–5 mGFAP-eGFP Tg mice to label the dividing eGFP+ cells. We monitored 180 eGFP+/HuKO+ cells and found 14 HuKO+ cells that lost eGFP expression during the observation period. At the end of the culture, all cells were positive for Hu and NeuroD, but negative for GFAP (Fig. 3). These results suggest that the majority of GFAP+ progenitors finally differentiated into Hu+/NeuroD+ neurons through a Hu+/GFAP+ transient state (Fig. 3).

Although the percentage of 2 GFAP+ cell pairs decreased as the culture time after cell division increased, half of the symmetrically divided eGFP+ cells were still positive for GFAP. These GFAP+ daughter cell pairs appear to be primary progenitor cells (self-renewing) and astrocytes (astrogliogenesis). As most of the GFAP+ symmetrically divided daughter cell pairs were also positive for nestin, a marker for progenitor cells (83.3%, Fig. 4). In addition, most eGFP+/GFAP+/Hu− cells also expressed another progenitor cell marker, Sox2 [34,35] in the P5 GFAP-eGFP mouse hippocampus (99.1% of a total of 113 cells; Figure S6) and both of the GFAP+/Hu− symmetrically divided daughter cells expressed Sox2 in the cultured slices (Figure S7), suggesting that the GFAP+/Hu− daughter cells may possess the properties of neurogenic primary progenitors. This is also supported by our previous studies showing that approximately 70% to 80% of progenitor cells of the early postnatal dentate gyrus become neurons *in vivo* [2]. To clarify whether or not the GFAP+ daughter cells are neurogenic progenitors, longer range time-lapse imaging is needed.

Fates of asymmetrically divided eGFP cells

In addition to symmetric cell division, less than 10% of eGFP+ cells divided asymmetrically and produced a GFAP+/Hu+ cell and a GFAP+ cell (Fig. 2A, Fig. 5, Video S3). This suggests the possibility that GFAP+ progenitor cells produced a cell pair consisting of a neuron-committed cell and a self-renewed GFAP+ cell by asymmetric cell division. However, we could not confirm if GFAP+/Hu+ cells finally developed into immature neurons that were positive only for neuronal markers, because of the decrease in eGFP expression in neuron-committed cells.

To examine the neuronal fate of daughter cells produced by asymmetric division of progenitor cells, nestin-GFP transgenic mice were used because nestin-eGFP is reportedly expressed by primary progenitors and the subsequent progenitors express only neuronal markers [13,36]. Of all nestin-eGFP+ dividing cells, 16.7% of eGFP+ cells divided asymmetrically and produced cell pairs consisting of an Hu+ cell and a GFAP+/nestin+ cell (n = 24 GFP+ cell pairs, Fig. 6, Video S4). These results suggest that asymmetric division of GFAP+ progenitors produced pairs of an immature neuron or neuronal progenitors, and a self-renewed GFAP+/nestin+ primary progenitor.

Discussion

Using time-lapse analysis with a slice culture of the postnatal hippocampus from mGFAP-eGFP Tg mice and nestin-eGFP Tg mice, we examined how GFP+ proliferating progenitors that

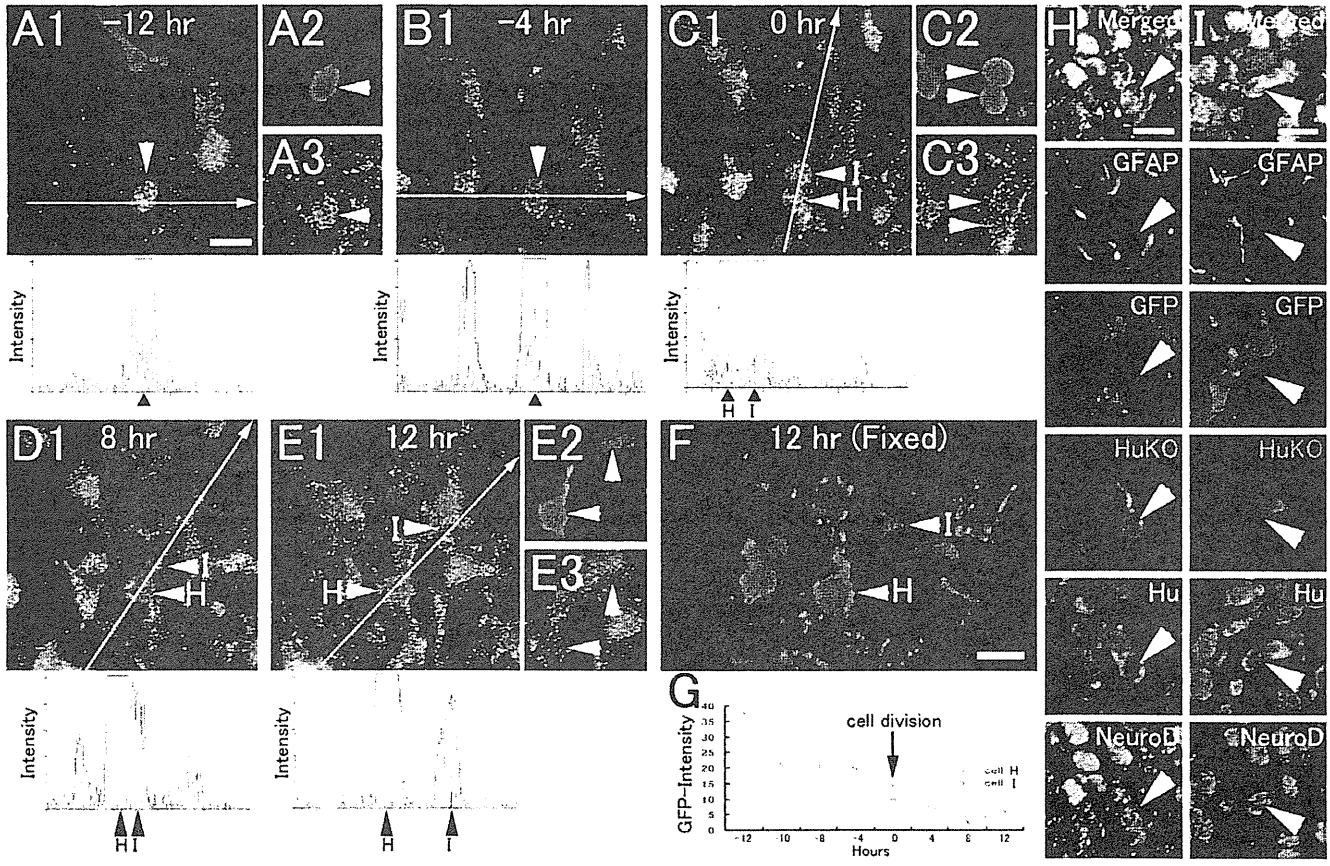

Figure 3. Symmetrical neuronal fate of GFAP+ progenitor cells. A–E, G: Time-lapse imaging of GFP+/HuKO+ cells. The eGFP signals (arrows) gradually decreased, and finally reached background level (A–E, G: fluorescent signal intensity chart). F: Optical images. H–I: Since each cell (arrowheads) in F was located at a different level of the Z-axis, the cells are shown separately in H and I. At the end of culture, both HuKO+ daughter cells expressed Hu and NeuroD. Scale bar, 10 μm.
doi:10.1371/journal.pone.0025303.g003

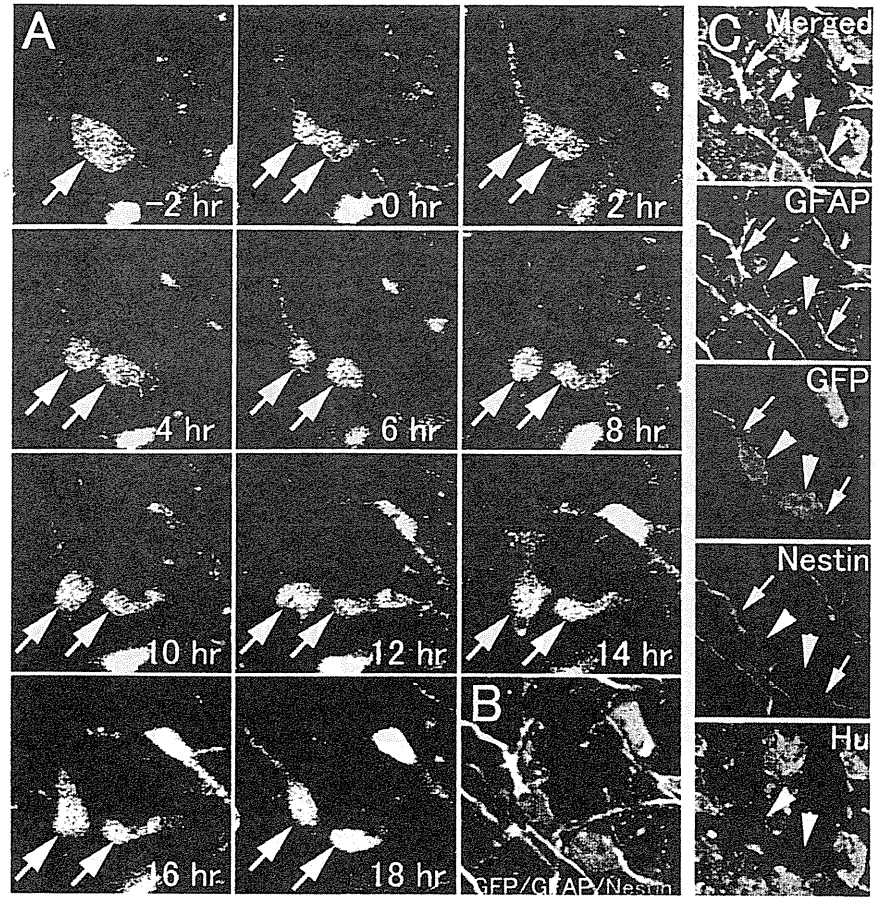

Figure 4. Symmetric division of eGFP+ cells to produce 2 GFAP+/nestin+ cells. A: Time-lapse imaging of GFP+ cell division in a hippocampal slice from a P6 GFAP-eGFP Tg mouse. B: 18 hours after cell division, the slice was fixed and then processed for immunohistochemistry. Optical images C: Both eGFP+ daughter cells (arrowheads) had a radial process and expressed an astrocytic cell marker (GFAP) and a progenitor cell marker (nestin) (arrows), suggesting the self-renewal of a progenitor cell.
doi:10.1371/journal.pone.0025303.g004

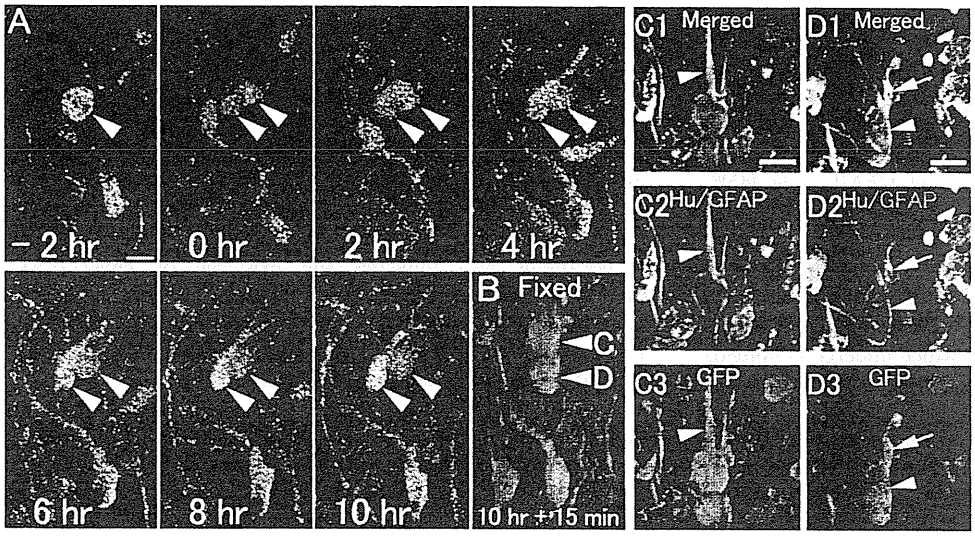

Figure 5. Asymmetric division of eGFP+ cells to produce a GFAP+ radial type cell and a neuronal cell. A: Time-lapse imaging of GFP+ cell division in a hippocampal slice from a P6 GFAP-eGFP Tg mouse. Also see Video S3. B: 10 hours after cell division, the slice was fixed and then processed for immunohistochemistry. Optical images (C, D): The cells in B indicated by arrowheads C and D are located at different levels of the Z-axis. Each cell is shown separately in different single optical images of C and D. The GFP-positive cells (arrowheads C and D) in B correspond to those indicated by arrowheads in C and D, respectively. One GFP+ daughter cell has a radial process and an astrocytic cell marker (GFAP+). Another GFP+ daughter cell expresses GFAP and the neuronal marker Hu, suggesting a neuronal lineage-commitment. Scale bar, 10 μm.
doi:10.1371/journal.pone.0025303.g005

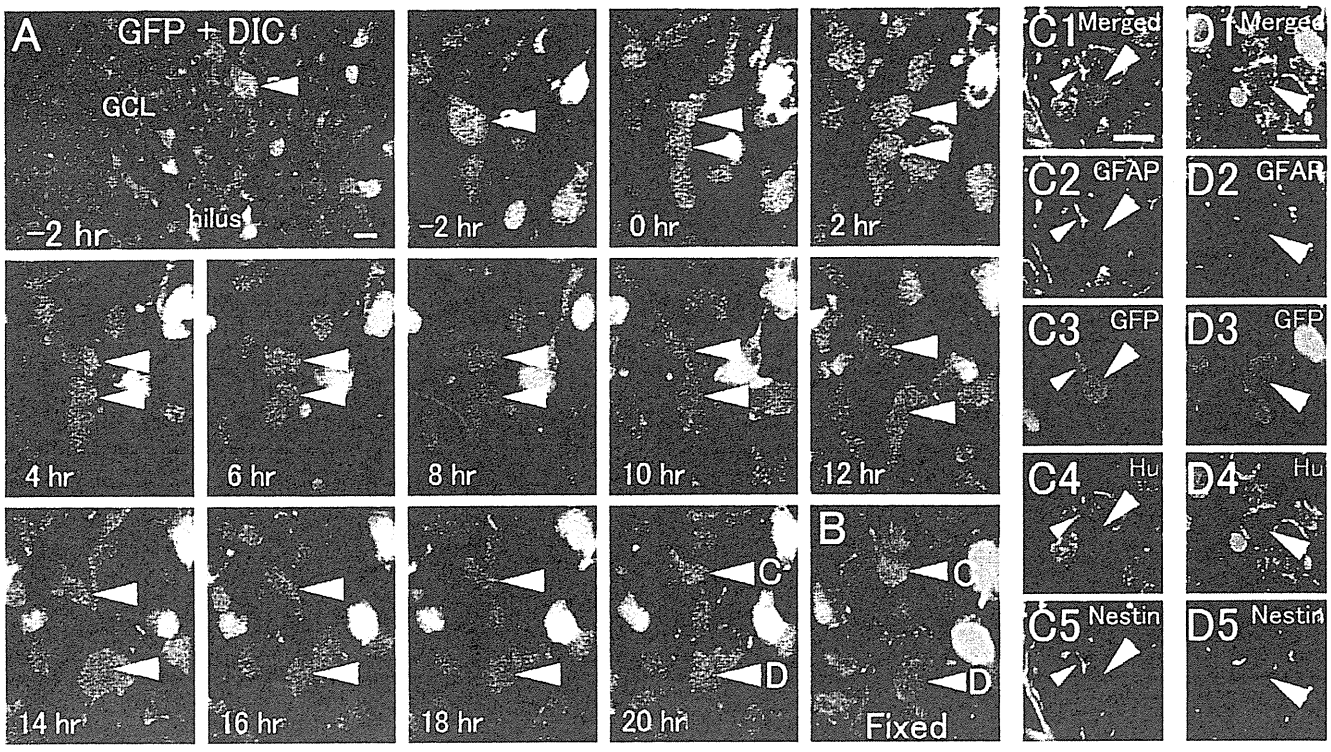

Figure 6. Asymmetric division of GFP+ cells to produce a GFAP+/nestin+ radial type cell and a neuronal cell. A: Time-lapse imaging of GFP+ cell division in a hippocampal slice from a P5 nestin-GFP Tg mouse (see Video S4). B: 20 hours after cell division, the slice was fixed and then processed for immunohistochemistry. Optical images (C, D): The cells in B indicated by arrowheads C and D are located at different levels of the Z-axis. Each cell is shown separately in different single optical images of C and D. The GFP-positive cells (arrowheads C and D) in B correspond to those indicated by arrowheads in C and D, respectively. One GFP+ daughter cell had a radial process and an astrocytic cell marker (GFAP+) and a progenitor cell marker (nestin+). Another GFP+ daughter cell expressed the neuronal marker Hu+, but was negative for GFAP and nestin, suggesting neuronal differentiation. Scale bar, 10 μm.
doi:10.1371/journal.pone.0025303.g006

express GFAP, Sox2 and nestin divide and differentiate into neuron-committed cells. The present time-lapse observation clearly demonstrated that the neurogenic region in the early postnatal dentate gyrus contained 2 distinct types of GFAP+ "neurogenic" progenitor cells, in addition to GFAP+ progenitors to be able to produce a pair of GFAP+ cells. Judging from the results of immunohistochemistry for GFAP and neuronal markers, the majority underwent symmetric division to produce a pair of neuron-committed cells (45%) or pairs of GFAP+ cells (45%), while a minority of GFAP+ neurogenic progenitors exhibited asymmetric cell division to produce a GFAP+ progenitor cell and a neuron-committed cell (10%; Fig. 7). To date, despite a lack of a time-lapse imaging analysis in postnatal hippocampal neurogenesis, GFAP+ progenitors have been generally considered to be stem cells or stem cell-like progenitors which undergo asymmetric cell division [13,18,19,20,37]. Unusually, the present time-lapse study has shown that most of the GFAP+ progenitors are not typical stem cells, but progenitors which divide symmetrically to generate a pair of neuronal progenitors or immature neurons, at least in the early postnatal dentate gyrus, although a small fraction of stem cell-like cells dividing asymmetrically also exist. Symmetric cell division in early dentate proliferating cells is supported by a recent paper using retrovirus labeling, although in which the astrocytic properties of the proliferating cells are not identified [38].

Additionally, the present time-lapse study showed that about half of GFP+ dividing cells became Hu+/GFAP+ cells. Most Hu+/GFAP+ cells exhibited Tbr2 expression and their proliferative activity was low, suggesting that the majority of Hu+/GFAP+ cells are on the way to further differentiation into the next neuron-committed cells. Furthermore, retrovirus-HuKO labeling approach revealed that when HuKO-labeled dividing cells lost GFP fluorescence, most of the labeled cells became Hu+/GFAP− neuronal cells. Therefore, the majority of Hu+/Tbr2+/GFAP+ cells appear to be a transient state when GFAP+ astrocytic progenitors differentiate into immature neurons or neuronal precursors, and a minority is likely to be intermediate progenitors that can further proliferate and produce immature neurons. In this regard, our previous immunohistochemical study in the adult hippocampus also indicates the existence of Hu+/GFAP+ proliferating cells [20,39]. However, the proliferative activity of adult Hu+/GFAP+ cells is relatively high, suggesting a difference in the property of Hu+/GFAP+ progenitors between early postnatal and adult stages, as mentioned later.

Glial fibrillary acidic protein-positive progenitors function as transient amplifying cells

The cell division pattern and fate of GFAP+ proliferating cells revealed by time-lapse imaging suggest the identity of GFAP+ progenitors in the early dentate neurogenic region. In neocortical development, time-lapse imaging analysis has precisely defined 2 types of progenitors: stem cells and amplifying cells. Stem cells produce single stem cells and single neuron-committed progenitors by asymmetric cell division, or self-renew by symmetric cell division. Transient amplifying cells (also referred to as intermediate progenitors) undergo symmetric cell division to produce a pair

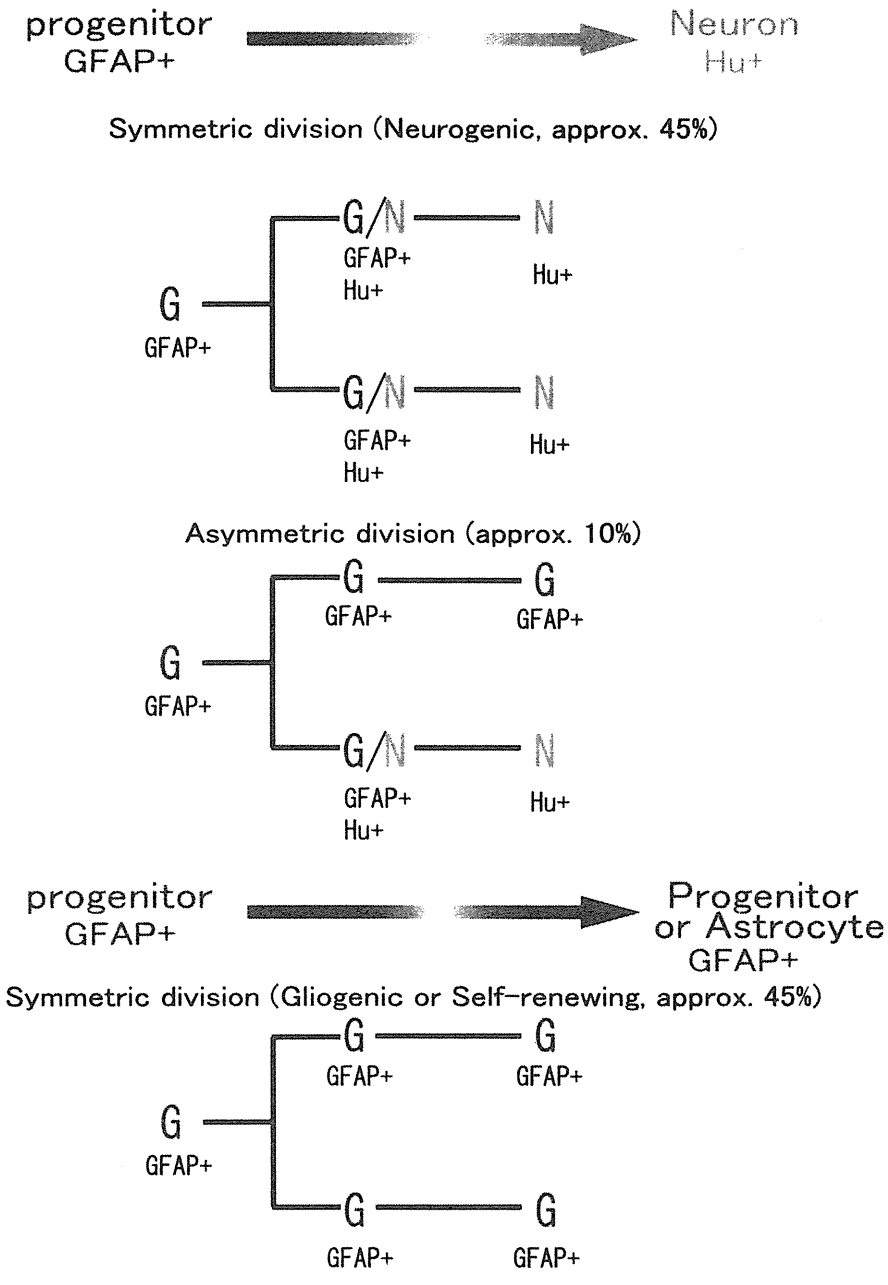

Figure 7. Diagram of cell division patterns of GFAP+ progenitors to produce dentate granule cells during the postnatal period. Most GFAP+ progenitor cells underwent symmetric division to generate neurons through an Hu+/GFAP+ transitional state, or to produce the neurons themselves. A small population of GFAP+ progenitor cells divided asymmetrically and produced both a self-renewed GFAP+ progenitor cell and a neuron.
doi:10.1371/journal.pone.0025303.g007

of neurons or self-renew [22,23,24]. According to the definition of neocortical progenitors, the majority of early postnatal dentate GFAP+ symmetrically dividing progenitors that produced a pair of neuron-committed progenitors or neurons can be identified as transient amplifying cells, while a minority of GFAP+ asymmetrically dividing progenitors appears to be stem cell-like progenitors. The neocortical amplifying cells are considered to play an important role in the increase in the number of neocortical neurons [40,41,42]. Similarly, the dentate GFAP+ transient amplifying progenitors would be required for the rapid production of dentate granule cells during the postnatal period [2,43,44,45].

However, we could not clearly define the nature of GFAP+ symmetrically dividing progenitors that produced a pair of GFAP+ cells. There appear to be various possible types of GFAP+ progenitors undergoing symmetrical proliferative division that are either 1) stem cell-like cells that divide during long periods, which self-renew and partially undergo asymmetric cell division; 2) neuron-committed transient amplifying cells that undergo a few or several symmetric divisions, and then produce neurons; or 3) astrocyte-committed transient amplifying cells that symmetrically divide a few or several times and subsequently generate astrocytes. Because astrocyte-like cells and proliferating cells in the postnatal

neurogenic zone exhibit an age-dependent decrease, and a majority of astrocyte-like proliferating cells become neurons [2,10], a majority of GFAP+ progenitors do not appear to be stem cells or gliogenic transient amplifying progenitors, but rather neuron-committed transient amplifying cells. However, there should be a small number which self-renew as stem cell-like cells and give rise to astrocytes. To accurately distinguish these GFAP+ progenitor cells, it is necessary to perform long-term cultures in time-lapse experiments to pursue the progeny of GFAP+ cells over several cell divisions. However, it may be difficult to perform such experiments, because our previous slice culture experiments suggest that the neurogenic capacity of dividing neural progenitors is reduced as the culture period becomes longer [21]. To maintain their capacity for neuronal differentiation, new hippocampal slice culture techniques in long-term time-lapse experiments are required.

Similarities and differences between postnatal and adult neurogenesis

A fundamental question is whether GFAP+ transient amplifying progenitors exist in the adult dentate neurogenic zone. In the adult hippocampus, GFAP+ progenitors have been typically classified as stem cells or primary progenitors, designated as Type 1 or B cells [12,13,36]. The following intermediate or transient amplifying cells are considered to be devoid of GFAP and express proneuronal proteins (mash1 and neurogenin2) and neuronal markers (Hu, PSA-NCAM, DCX, NeuroD and Tbr2), designated as Type 2–3 or D cells [13,18,19,20]. Additionally, because adult GFAP+ progenitors have been speculated to be slowly dividing stem cells which divide asymmetrically [13,46], the adult SGZ does not appear to contain GFAP+ amplifying cells. However, it should be noted that the concept was mostly based on studies using BrdU-labeling and immunolabeling with glial and neuronal markers.

Several lines of evidence support the notion that the adult hippocampus also contains GFAP+ symmetrically dividing or amplifying neurogenic progenitors. Firstly, our previous studies in rats and GFAP-eGFP transgenic mice have shown that the adult neurogenic zone has 2 types of GFAP+ progenitors with or without neuronal (and proneuronal) markers such as Hu and Mash-1, in addition to the stem cell marker Sox2. The neuronal marker-positive progenitors have relatively higher proliferative activity and partial non-radial morphology, and do not appear to be stem cells, but rather amplifying progenitors [20,39]. Secondly, several studies have shown an increase in the number of GFAP+ neural progenitors in normal, enriched, running [47], seizure-induced [48] and N-methyl-D-aspartate receptor antagonist-treated animals [49,50], suggesting symmetric cell division of GFAP+ progenitors since their number will not increase with only asymmetric cell division. Finally, a time course experiment of BrdU-labeled progenitors demonstrates that the increase in the number of GFAP+ progenitors is transient [47]. After an increase in the number of the GFAP+/BrdU+ progenitors, a gradual decrease begins, while the number of neuronal marker-expressing BrdU+ cells increases. This apparently indicates that a daughter cell pair of GFAP+ progenitors becomes neurons, because the number of the GFAP+/BrdU+ progenitors never decreases by only asymmetric cell division. Taken together, these data strongly suggest that the GFAP+ neural progenitors, owing to their transient increase, principally function as transient amplifying progenitors to produce neurons in the adult hippocampus in addition to their role in neural and glial stem cells, as suggested previously [47].

Although these studies suggest the presence of GFAP+ amplifying progenitors from the early postnatal to adult hippocampus, it should also be noted that there could be some differences in the properties of GFAP+ amplifying cells between the two stages. For example, major GFAP+ proliferating cells were Hu-negative in the early postnatal dentate neurogenic regions, but Hu-positive in the adult ones [2,20,39]. A study using the neurosphere assay has shown that progenitor cells from the early

Table 1. Antibodies.

Marker	Species, isotype	Label	Working dilution	Vendor
Primary antibodies				
GFAP	Guinea pig IgG	None	1:800	Advanced ImmunoChem., CA, USA
GFP	Rat IgG	None	1:400	Nakalai Tesque, Japan
Hu	Human IgG	None	1:2000	Gift from Dr. H. J. Okano
Ki67	Mouse IgG	None	1:100	Novocastra, UK
Nestin	Mouse IgG	None	1:2000	BD Bioscience, CA, USA
NeuroD	Goat IgG	None	1:400	Santa Cruz Biotech., CA, USA
Sox2	Rabbit IgG	None	1:1000	Chemicon, CA, USA
Tbr2	Rabbit IgG	None	1:2000	Gift from Dr. R. Hevner
Secondary antibodies				
Anti-goat IgG	Donkey IgG	Cy5	1:200	Jackson, PA, USA
Anti-guinea pig IgG	Donkey IgG	Cy3	1:200	Jackson
Anti-guinea pig IgG	Donkey IgG	Biotin	1:200	Jackson
Anti-human IgG	Donkey IgG	Cy5	1:200	Jackson
Anti-mouse IgG	Donkey IgG	Cy5	1:200	Jackson
Anti-mouse IgG	Donkey IgG	Biotin	1:200	Jackson
Anti-rabbit IgG	Donkey IgG	Cy3	1:200	Jackson
Anti-rat IgG	Donkey IgG	Cy2	1:200	Jackson

doi:10.1371/journal.pone.0025303.t001

postnatal dentate gyrus exhibit self-renewal and multipotentiality, but those from the adult dentate gyrus rarely do [51]. It is thus possible that the early postnatal type of Hu−/GFAP+ amplifying progenitors progressively become adult-type Hu+/GFAP+ amplifying progenitors with aging, and that the alternation in the GFAP+ progenitors is associated with age-dependent decrease in postnatal neurogenesis [2,52,53,54]. Further investigation to reveal the mechanism underlying the regulation of cell division patterns and the age-dependent transition of GFAP+ amplifying progenitors will contribute to regenerative brain therapy, particularly regarding the up-regulation of intrinsic postnatal neurogenesis.

Materials and Methods

Animals and retroviral injection

All animal studies were approved by the Institutional Animal Care and Use Committee of Juntendo University, Japan. Before conducting any experiments, mGFAP-eGFP or nestin-GFP [55] transgenic mice were deeply anesthetized on ice. To trace newly generated cells, we used our modified retrovirus vector, GCDNsap-humanized Kusabira Orange (HuKO). Details of the construction and titer of this vector have been described previously [56]. For dual-color time-lapse imaging, a retrovirus vector (0.5 μl) was stereotactically injected into the hilus of P3–5 mGFAP-eGFP mice (posterior = 1 mm from the bregma; lateral = 1 mm; ventral = 1 mm), as described previously [2] and time-lapse imaging was scheduled for 2 days after the injection.

Slice culture preparation

Mice were deeply anesthetized on ice. Hippocampal slices were prepared by the standard method [21], and then the slices (350 μm in thickness) were transferred onto a collagen-coated glass bottom dish. The culture medium was a mixture of 50% minimum essential medium (Invitrogen, Carlsbad, CA, USA), 25% heat inactivated horse serum (Invitrogen) and 25% Hank's balanced salt solution (Invitrogen) supplemented with penicillin-streptomycin-glutamine (Invitrogen). Glucose was added to reach the final concentration of 6.5 mg/ml.

Time-lapse confocal imaging

Two to 3 hours after hippocampal slice preparation, time-lapse recording was performed manually using an inverted confocal laser scanning microscope (LSM 510 META; Zeiss, Germany) and minimal laser excitation (typically 1% of an Argon 488 laser) to prevent photodamage and photobleaching. Differential interference contrast images were obtained to confirm the granule cell layer. To monitor cell movements, stacks of images were collected in the z-plane every 2 or 4 hours using a 40× objective. Between these time points, slices were kept in a water-jacketed incubator at 34°C, with 5% CO_2 and 50% O_2. After time-lapse imaging, cultured slices were fixed overnight in a 4% paraformaldehyde solution at 4°C. Time-lapse sequences were arranged using Photoshop (Adobe Systems Inc., CA, USA) and QuickTime Pro (Apple, Cupertino, CA, USA).

Quantification of GFP expression in HuKO-labeled cells

To quantify the expression levels of GFP in HuKO-labeled cells, we randomly chose 180 GFP+/HuKO+ cells. The average fluorescence intensities of GFP were calculated using Image-J software. Microscope settings, such as laser power, pinhole size and detector gain, were kept equivalent during time-lapse imaging.

Immunofluorescence staining of time-lapse imaged slices

The antibodies, concentrations and vendors used are listed in Table 1. Fixed slices were washed with phosphate-buffered saline (PBS). The primary antibodies were diluted with PBS containing 1% bovine serum albumin (BSA), 0.2% Triton X-100 and 10% normal donkey serum, and the secondary antibodies were diluted with PBS containing 1% BSA, 0.1% Triton X-100 and 1% normal donkey serum. All subsequent incubations were carried out with free-floating sections in 10-ml vials using a rotator. Each of the following steps was followed by PBS washing: the slices were incubated overnight for 3 days with a mixture of primary antibodies diluted in the same solution at 4°C. The sections were then incubated at room temperature for 3 hours with a mixture of secondary antibodies. The slices were further incubated at room temperature for 3 hours with streptavidin-Alexa 405 (Invitrogen) (1:400). Finally, the specimens were mounted on glass slides. For quintuple staining, Cy5 signals were completely photobleached under LSM 510 META (Zeiss) after quadruple imaging, as described below. The slices were then washed with PBS and incubated overnight for 3 days with goat anti-NeuroD diluted in PBS containing 1% BSA, 0.2% Triton X-100 and 10% normal donkey serum at 4°C. The sections were then incubated at room temperature for 3 hours with donkey anti-goat IgG-Cy5. Finally, the specimens were remounted on glass slides. Samples were viewed through LSM 510 META (Zeiss) with 20× and 63× objectives. The images were corrected for brightness and contrast using the Zeiss LSM Image Browser, Adobe Illustrator 9.0 (Adobe Systems Inc.) and Adobe Photoshop 7.0 (Adobe Systems Inc.)

Immunofluorescence staining of fixed hippocampal tissues

Immunohistochemistry was performed as described previously [2]. Briefly, the frozen brains were coronally sliced into 14-μm sections using a cryostat (CM-3000; Leica, Nussloch, Germany). After washing in PBS, the sections were incubated at 4°C overnight with first antibodies in PBS containing 1% bovine serum albumin (BSA), then incubated at room temperature for 1–2 h with secondary antibodies in PBS containing 1% BSA. For immunostaining with anti-Tbr2 antibody, the sections were boiled in 0.01 M citrate buffer for 15 min and washed in PBS prior to the first antibody incubation.

Statistical analysis

For comparison of 2 groups, statistical significance was assessed using the chi-square test or Mann-Whitney U test. A total of 79 GFAP-eGFP+ daughter cell pairs were counted.

Supporting Information

Figure S1 Schematic illustration of time-lapse imaging analysis. Images are collected in cultured hippocampal slices every two hours. The time at which one eGFP+ cell divides into two daughter cells is regarded as time zero (0 hours). For example, if an eGFP+ cell divides into two daughter cells 12 hours after culture and the slice is fixed 28 hours, this is depicted as "16 hours after cell division".
(TIF)

Figure S2 Quadruple staining of eGFP+ daughter cells at 0 hours after cell division. eGFP+ cells indicated by arrowheads correspond to the cells in Fig. 1B. Both daughter cells (arrowheads) expressed GFAP and nestin, but not Hu.
(TIF)

Figure S3 Time-lapse imaging of eGFP+ cells (A) and daughter cell fates at the end of culture (B, C). A: Full time-scale images of eGFP+ cells represented in Fig. 1C. B, C: Two eGFP+ daughter cells at the end of imaging. Both daughter cells expressed GFAP (magenta), but not Hu (blue).
(TIF)

Figure S4 Time-lapse imaging of eGFP+ cells (A) and daughter cell fates at the end of culture (B, C). A: Full time-scale images of eGFP+ cells are represented in Fig. 1D. B, C, D: Two eGFP+ daughter cells at the end of the imaging. Both daughter cells expressed GFAP (magenta) and Hu (blue).
(TIF)

Figure S5 Phenotypic analysis of eGFP+ cells in the dentate gyrus at P5. The eGFP+ (green)/GFAP+ (white)/Hu+ (blue) cell indicated by arrow is also positive for Tbr2 (magenta). Scale bar, 5 μm.
(TIF)

Figure S6 Phenotypic analysis of eGFP+ cells in the dentate gyrus at P5. The eGFP+ (green)/GFAP+ (white)/Hu− (blue) cells indicated by arrows are also positive for Sox2 (magenta). Scale bar, 10 μm.
(TIF)

Figure S7 Symmetric division of eGFP+ cells to produce 2 GFAP+/Sox2+ cells. A, B: Time-lapse imaging of GFP+ cell division in a hippocampal slice from a P4 GFAP-eGFP Tg mouse. C: Both eGFP+ daughter cells (arrowheads) expressed an astrocytic cell marker (GFAP) and a progenitor cell marker (Sox2), suggesting the self-renewal of a progenitor cell. Scale bar, 5 μm.
(TIF)

Video S1 Time-lapse video of GFAP-eGFP+ cells shown in Fig. 2D and Figure S3. Arrowheads indicate the eGFP+ mother cell and daughter cells.
(AVI)

Video S2 Time-lapse video of GFAP-eGFP+ cells shown in Fig. 2E and Figure S4. Arrowheads indicate eGFP+ daughter cells.
(AVI)

Video S3 Time-lapse video of GFAP-eGFP+ cells shown in Fig. 5. Arrowheads indicate the eGFP+ mother cell and daughter cells.
(AVI)

Video S4 Time-lapse video of nestin-GFP+ cells shown in Fig. 6. Arrowheads indicate the GFP+ mother cell and daughter cells.
(AVI)

Acknowledgments

We are very grateful to Dr. Hirotaka J. Okano of Keio University, Dr. Robert B. Darnell of Rockefeller University for the anti-Hu antibody and Dr. Robert F. Hevner of the University of Washington for the anti-Tbr2 antibody. We also appreciate the editorial review of the manuscript by Mr. Roderick J. Turner, Assistant Professor Edward F. Barroga and J. Patrick Barron, Professor and Chair of the Department of International Medical Communications, Tokyo Medical University.

Author Contributions

Conceived and designed the experiments: TN TS. Performed the experiments: TN. Analyzed the data: TN. Contributed reagents/materials/analysis tools: HM RS MO MY HN SS. Wrote the paper: TN TS.

References

1. Altman J, Bayer SA (1990) Migration and distribution of two populations of hippocampal granule cell precursors during the perinatal and postnatal periods. J Comp Neurol 301: 365–381.
2. Namba T, Mochizuki H, Onodera M, Mizuno Y, Namiki H, et al. (2005) The fate of neural progenitor cells expressing astrocytic and radial glial markers in the postnatal rat dentate gyrus. Eur J Neurosci 22: 1928–1941.
3. Seki T, Arai Y (1993) Highly polysialylated neural cell adhesion molecule (NCAM-H) is expressed by newly generated granule cells in the dentate gyrus of the adult rat. J Neurosci 13: 2351–2358.
4. Ming GL, Song H (2005) Adult neurogenesis in the mammalian central nervous system. Annu Rev Neurosci 28: 223–250.
5. Parent JM, Yu TW, Leibowitz RT, Geschwind DH, Sloviter RS, et al. (1997) Dentate granule cell neurogenesis is increased by seizures and contributes to aberrant network reorganization in the adult rat hippocampus. J Neurosci 17: 3727–3738.
6. Sahay A, Hen R (2007) Adult hippocampal neurogenesis in depression. Nat Neurosci 10: 1110–1115.
7. Zhao C, Deng W, Gage FH (2008) Mechanisms and functional implications of adult neurogenesis. Cell 132: 645–660.
8. Dranovsky A, Hen R (2006) Hippocampal neurogenesis: regulation by stress and antidepressants. Biol Psychiatry 59: 1136–1143.
9. Eisch AJ, Cameron HA, Encinas JM, Meltzer LA, Ming GL, et al. (2008) Adult neurogenesis, mental health, and mental illness: hope or hype? J Neurosci 28: 11785–11791.
10. Ganat YM, Silbereis J, Cave C, Ngu H, Anderson GM, et al. (2006) Early postnatal astroglial cells produce multilineage precursors and neural stem cells in vivo. J Neurosci 26: 8609–8621.
11. Garcia AD, Doan NB, Imura T, Bush TG, Sofroniew MV (2004) GFAP-expressing progenitors are the principal source of constitutive neurogenesis in adult mouse forebrain. Nat Neurosci 7: 1233–1241.
12. Seri B, Garcia-Verdugo JM, McEwen BS, Alvarez-Buylla A (2001) Astrocytes give rise to new neurons in the adult mammalian hippocampus. J Neurosci 21: 7153–7160.
13. Kempermann G, Jessberger S, Steiner B, Kronenberg G (2004) Milestones of neuronal development in the adult hippocampus. Trends Neurosci 27: 447–452.
14. Alvarez-Buylla A, Seri B, Doetsch F (2002) Identification of neural stem cells in the adult vertebrate brain. Brain Res Bull 57: 751–758.
15. Lagace DC, Whitman MC, Noonan MA, Ables JL, DeCarolis NA, et al. (2007) Dynamic contribution of nestin-expressing stem cells to adult neurogenesis. J Neurosci 27: 12623–12629.
16. Imayoshi I, Sakamoto M, Ohtsuka T, Takao K, Miyakawa T, et al. (2008) Roles of continuous neurogenesis in the structural and functional integrity of the adult forebrain. Nat Neurosci 11: 1153–1161.
17. Ninkovic J, Mori T, Gotz M (2007) Distinct modes of neuron addition in adult mouse neurogenesis. J Neurosci 27: 10906–10911.
18. Ozen I, Galichet C, Watts C, Parras C, Guillemot F, et al. (2007) Proliferating neuronal progenitors in the postnatal hippocampus transiently express the proneural gene Ngn2. Eur J Neurosci 25: 2591–2603.
19. Hodge RD, Kowalczyk TD, Wolf SA, Encinas JM, Rippey C, et al. (2008) Intermediate progenitors in adult hippocampal neurogenesis: Tbr2 expression and coordinate regulation of neuronal output. J Neurosci 28: 3707–3717.
20. Seki T, Namba T, Mochizuki H, Onodera M (2007) Clustering, migration, and neurite formation of neural precursor cells in the adult rat hippocampus. J Comp Neurol 502: 275–290.
21. Namba T, Mochizuki H, Onodera M, Namiki H, Seki T (2007) Postnatal neurogenesis in hippocampal slice cultures: early in vitro labeling of neural precursor cells leads to efficient neuronal production. J Neurosci Res 85: 1704–1712.
22. Miyata T, Kawaguchi A, Saito K, Kawano M, Muto T, et al. (2004) Asymmetric production of surface-dividing and non-surface-dividing cortical progenitor cells. Development 131: 3133–3145.
23. Noctor SC, Martinez-Cerdeno V, Ivic L, Kriegstein AR (2004) Cortical neurons arise in symmetric and asymmetric division zones and migrate through specific phases. Nat Neurosci 7: 136–144.
24. Haubensak W, Attardo A, Denk W, Huttner WB (2004) Neurons arise in the basal neuroepithelium of the early mammalian telencephalon: a major site of neurogenesis. Proc Natl Acad Sci U S A 101: 3196–3201.
25. Suzuki R, Arata S, Nakajo S, Ikenaka K, Kikuyama S, et al. (2003) Expression of the receptor for pituitary adenylate cyclase-activating polypeptide (PAC1-R) in reactive astrocytes. Brain Res Mol Brain Res 115: 10–20.
26. Gahwiler BH, Capogna M, Debanne D, McKinney RA, Thompson SM (1997) Organotypic slice cultures: a technique has come of age. Trends Neurosci 20: 471–477.
27. Raineteau O, Hugel S, Ozen I, Rietschin L, Sigrist M, et al. (2006) Conditional labeling of newborn granule cells to visualize their integration into established circuits in hippocampal slice cultures. Mol Cell Neurosci 32: 344–355.
28. Kamada M, Li RY, Hashimoto M, Kakuda M, Okada H, et al. (2004) Intrinsic and spontaneous neurogenesis in the postnatal slice culture of rat hippocampus. Eur J Neurosci 20: 2499–2508.

29. Raineteau O, Rietschin L, Gradwohl G, Guillemot F, Gahwiler BH (2004) Neurogenesis in hippocampal slice cultures. Mol Cell Neurosci 26: 241–250.
30. Stoppini L, Buchs PA, Muller D (1991) A simple method for organotypic cultures of nervous tissue. J Neurosci Methods 37: 173–182.
31. Nowakowski RS, Lewin SB, Miller MW (1989) Bromodeoxyuridine immunohistochemical determination of the lengths of the cell cycle and the DNA-synthetic phase for an anatomically defined population. J Neurocytol 18: 311–318.
32. Cameron HA, McKay RD (2001) Adult neurogenesis produces a large pool of new granule cells in the dentate gyrus. J Comp Neurol 435: 406–417.
33. Hevner RF, Hodge RD, Daza RA, Englund C (2006) Transcription factors in glutamatergic neurogenesis: conserved programs in neocortex, cerebellum, and adult hippocampus. Neurosci Res 55: 223–233.
34. Hodge RD, Hevner RF (2011) Expression and actions of transcription factors in adult hippocampal neurogenesis. Dev Neurobiol 71: 680–689.
35. Suh H, Consiglio A, Ray J, Sawai T, D'Amour KA, et al. (2007) In vivo fate analysis reveals the multipotent and self-renewal capacities of Sox2+ neural stem cells in the adult hippocampus. Cell Stem Cell 1: 515–528.
36. Fukuda S, Kato F, Tozuka Y, Yamaguchi M, Miyamoto Y, et al. (2003) Two distinct subpopulations of nestin-positive cells in adult mouse dentate gyrus. J Neurosci 23: 9357–9366.
37. Encinas JM, Michurina TV, Peunova N, Park JH, Tordo J, et al. (2011) Division-coupled astrocytic differentiation and age-related depletion of neural stem cells in the adult hippocampus. Cell Stem Cell 8: 566–579.
38. Yokose J, Ishizuka T, Yoshida T, Aoki J, Koyanagi Y, et al. (2011) Lineage analysis of newly generated neurons in organotypic culture of rat hippocampus. Neurosci Res 69: 223–233.
39. Liu Y, Namba T, Liu J, Suzuki R, Shioda S, et al. (2010) Glial fibrillary acidic protein-expressing neural progenitors give rise to immature neurons via early intermediate progenitors expressing both glial fibrillary acidic protein and neuronal markers in the adult hippocampus. Neuroscience 166: 241–251.
40. Fish JL, Dehay C, Kennedy H, Huttner WB (2008) Making bigger brains-the evolution of neural-progenitor-cell division. J Cell Sci 121: 2783–2793.
41. Kriegstein A, Noctor S, Martinez-Cerdeno V (2006) Patterns of neural stem and progenitor cell division may underlie evolutionary cortical expansion. Nat Rev Neurosci 7: 883–890.
42. Noctor SC, Martinez-Cerdeno V, Kriegstein AR (2007) Contribution of intermediate progenitor cells to cortical histogenesis. Arch Neurol 64: 639–642.
43. Bayer SA (1980) Development of the hippocampal region in the rat. I. Neurogenesis examined with 3H-thymidine autoradiography. J Comp Neurol 190: 87–114.
44. Schlessinger AR, Cowan WM, Gottlieb DI (1975) An autoradiographic study of the time of origin and the pattern of granule cell migration in the dentate gyrus of the rat. J Comp Neurol 159: 149–175.
45. Muramatsu R, Ikegaya Y, Matsuki N, Koyama R (2007) Neonatally born granule cells numerically dominate adult mice dentate gyrus. Neuroscience 148: 593–598.
46. Malatesta P, Hack MA, Hartfuss E, Kettenmann H, Klinkert W, et al. (2003) Neuronal or glial progeny: regional differences in radial glia fate. Neuron 37: 751–764.
47. Steiner B, Kronenberg G, Jessberger S, Brandt MD, Reuter K, et al. (2004) Differential regulation of gliogenesis in the context of adult hippocampal neurogenesis in mice. Glia 46: 41–52.
48. Huttmann K, Sadgrove M, Wallraff A, Hinterkeuser S, Kirchhoff F, et al. (2003) Seizures preferentially stimulate proliferation of radial glia-like astrocytes in the adult dentate gyrus: functional and immunocytochemical analysis. Eur J Neurosci 18: 2769–2778.
49. Nacher J, Rosell DR, Alonso-Llosa G, McEwen BS (2001) NMDA receptor antagonist treatment induces a long-lasting increase in the number of proliferating cells, PSA-NCAM-immunoreactive granule neurons and radial glia in the adult rat dentate gyrus. Eur J Neurosci 13: 512–520.
50. Namba T, Maekawa M, Yuasa S, Kohsaka S, Uchino S (2009) The Alzheimer's disease drug memantine increases the number of radial glia-like progenitor cells in adult hippocampus. Glia 57: 1082–1090.
51. Seaberg RM, van der Kooy D (2002) Adult rodent neurogenic regions: the ventricular subependyma contains neural stem cells, but the dentate gyrus contains restricted progenitors. J Neurosci 22: 1784–1793.
52. Kuhn HG, Dickinson-Anson H, Gage FH (1996) Neurogenesis in the dentate gyrus of the adult rat: age-related decrease of neuronal progenitor proliferation. J Neurosci 16: 2027–2033.
53. Mathews EA, Morgenstern NA, Piatti VC, Zhao C, Jessberger S, et al. (2010) A distinctive layering pattern of mouse dentate granule cells is generated by developmental and adult neurogenesis. J Comp Neurol 518: 4479–4490.
54. Seki T, Arai Y (1995) Age-related production of new granule cells in the adult dentate gyrus. Neuroreport 6: 2479–2482.
55. Yamaguchi M, Saito H, Suzuki M, Mori K (2000) Visualization of neurogenesis in the central nervous system using nestin promoter-GFP transgenic mice. Neuroreport 11: 1991–1996.
56. Suzuki A, Obi K, Urabe T, Hayakawa H, Yamada M, et al. (2002) Feasibility of ex vivo gene therapy for neurological disorders using the new retroviral vector GCDNsap packaged in the vesicular stomatitis virus G protein. J Neurochem 82: 953–960.

Cytokine 55 (2011) 402–408

Contents lists available at ScienceDirect

Cytokine

journal homepage: www.elsevier.com/locate/issn/10434666

Growth promotion of genetically modified hematopoietic progenitors using an antibody/c-Mpl chimera

Masahiro Kawahara [a,*], Jianhong Chen [a], Takahiro Sogo [a], Jinying Teng [a], Makoto Otsu [b], Masafumi Onodera [c], Hiromitsu Nakauchi [b], Hiroshi Ueda [a], Teruyuki Nagamune [a]

[a] Department of Chemistry and Biotechnology, School of Engineering, The University of Tokyo, 7-3-1 Hongo, Bunkyo-ku, Tokyo 113-8656, Japan
[b] Division of Stem Cell Therapy, Center for Stem Cell Biology and Regenerative Medicine, Institute of Medical Science, The University of Tokyo, 4-6-1, Shirokanedai, Minato-ku, Tokyo 108-8639, Japan
[c] Department of Genetics, National Research Institute for Child Health and Development, 2-10-1 Okura, Setagaya-ku, Tokyo 157-8535, Japan

ARTICLE INFO

Article history:
Received 29 December 2010
Accepted 27 May 2011
Available online 22 June 2011

Keywords:
Antibody
Chimeric protein
Cytokine receptor
Hematopoietic stem cell
Signal transduction

ABSTRACT

Thrombopoietin is a potent cytokine that exerts proliferation of hematopoietic stem cells (HSCs) through its cognate receptor, c-Mpl. Therefore, mimicry of c-Mpl signaling by a receptor recognizing an artificial ligand would be attractive to attain specific expansion of genetically modified HSCs. Here we propose a system enabling selective expansion of genetically modified cells using an antibody/receptor chimera that can be activated by a specific antigen. We constructed an antibody/c-Mpl chimera, in which single-chain Fv (ScFv) of an anti-fluorescein antibody was tethered to the extracellular D2 domain of the erythropoietin receptor and transmembrane/cytoplasmic domains of c-Mpl. When the chimera was expressed in interleukin (IL)-3-dependent pro-B cell line Ba/F3, genetically modified cells were selectively expanded in the presence of fluorescein-conjugated BSA (BSA-FL) as a specific antigen. Furthermore, highly purified mouse HSCs transduced with the retrovirus carrying antibody/c-Mpl chimera gene proliferated in vitro in response to BSA-FL, and the cells retained in vivo long-term repopulating abilities. These results demonstrate that the antibody/c-Mpl chimera is capable of signal transduction that mimics wild-type c-Mpl signaling.

1. Introduction

Cytokines are small secreted proteins that regulate various cellular fates including proliferation, differentiation and death. Cytokines bind to their cognate receptors expressed on the target cell surface, triggering activation of the receptors and initiating downstream signaling cascades. Although ligand-induced dimerization has been considered as a key event in the activation of cytokine receptors, increasing evidences suggest that conformational change is another key event in the activation of cytokine receptors. Crystallographic analyses of the erythropoietin receptor (EpoR), which is a member of the type I cytokine receptor superfamily, clearly revealed that EpoR exists as a preformed dimer even in the absence of ligand [1]. Additionally the same study showed that ligand binding to the extracellular D1 domain brings the intracellular domains of two receptor chains into close proximity, in which the conformation of the receptor is switched to an active state. This model was also supported by biochemical analyses, such as fluorescence resonance energy transfer (FRET) assays [2–4], dihydrofolate reductase (DHFR) [5] and β-galactosidase complementation assays [6].

Besides molecular analyses of the cytokine receptor system, mimicry of cytokine functions with artificial ligands would be a promising strategy for realizing artificial control of the fates of specific cell populations. To this end, we have designed several antibody/cytokine receptor chimeras that can transduce a growth signal in response to a cognate antigen. An anti-fluorescein single-chain Fv (ScFv) fused to the extracellular D2 domain of EpoR was joined to the transmembrane and cytoplasmic domains of EpoR, gp130, IL-2R, epidermal growth factor receptor (EGFR) and c-Fms to create a series of antibody/receptor chimeras. When IL-3-dependent murine pro-B cell line Ba/F3 was transduced with each antibody/receptor chimera, fluorescein-conjugated BSA (BSA-FL) induced oligomerization of chimeric receptors, enabling cell growth in the medium containing BSA-FL but without IL-3 [7–11]. In addition, these chimeric receptors were able to specifically amplify gene-transduced cells in an antigen-dependent manner (antigen-mediated genetically modified cell amplification, AMEGA) [7–11].

Although the antibody/receptor chimeras have been shown to work in cultured cell lines including pro-B (Ba/F3) [7–11], myeloid

* Corresponding author. Tel.: +81 3 5841 7356; fax: +81 3 5841 8657.
E-mail address: kawahara@bio.t.u-tokyo.ac.jp (M. Kawahara).

1043-4666/$ - see front matter © 2011 Elsevier Ltd. All rights reserved.
doi:10.1016/j.cyto.2011.05.024

(FDC-P1) [12], hybridoma (7TD1) [13], mouse embryonic fibroblast (NIH3T3) [11] and IL-2-dependent T (CTLL-2) [10] cells, it has not been thoroughly investigated whether the antibody/receptor chimeras could also be applied to primary cells, except the demonstration in mouse splenic T cells [10]. In this study, we sought to apply this chimeric receptor system to hematopoietic stem cells (HSCs), which represent an invaluable cellular source for transplantation medicine. To this end, we replaced the cytoplasmic domain of the fluorescein-responsive antibody/receptor chimera with that of c-Mpl to construct an antibody/c-Mpl chimera, because the c-Mpl ligand, thrombopoietin (TPO), is known as a potent cytokine for proliferation of HSCs [14]. We investigated whether the antibody/c-Mpl chimera could be functional in Ba/F3 cells as a hematopoietic cell model and in highly purified mouse HSCs.

2. Materials and methods

2.1. Vector construction

The cDNA encoding transmembrane and cytoplasmic domains of human c-Mpl was obtained by RT-PCR using two primers (c-Mpl sense: 5'-GCCGATATCATCTCCTTGGTGACCGCTCTG-3' and c-Mpl antisense: 5'-GCCGGATCCTCAAGGCTGCTGCCAATAGCT-3') and total RNA of TF-1 cells (kindly provided from Dr. P.C. Wang, University of Tsukuba, Tsukuba, Japan) as a template. The cDNA fragment of human c-Mpl was digested with *Eco*RV and *Bam*HI, and subcloned into pBluescript II-SK(−) (Stratagene, La Jolla, CA) digested with the same enzymes to make pBS-c-Mpl, followed by confirmation of the sequence. pBS-c-Mpl was digested with *Eco*RV and *Bam*HI, and ligated to *Eco*RV–*Bam*HI-digested pBS-ED2-IG [13] encoding the D2 domain of the human EpoR, internal ribosomal entry site (IRES) and enhanced green fluorescent protein (EGFP) to make pBS-EMpl-IG. pBS-EMpl-IG was digested with *Bam*HI and *Bsp*EI, and inserted into pMK-SEγ-IG [10] digested with the same enzymes, resulting in pMK-S-Mpl-IG. To create a pGCDNsam-based retroviral expression vector, pMK-S-Mpl-IG was digested with *Bam*HI and *Xba*I, and inserted into pBluescript II-SK(−) digested with the same enzymes, resulting in pBS-SEMpl. pBS-SEMpl was digested with *Bam*HI and *Not*I, and subcloned into pGCDNsam-I/E [15–17] to create pGCDNsam-S-Mpl-I/E.

2.2. Animals and cell lines

C57BL/6-Ly5.1 and C57BL/6-Ly5.2 mice were purchased from Japan SLC (Shizuoka, Japan). C57BL/6-Ly5.1/Ly5.2 F1 mice were bred and maintained in the Animal Research Facility of the Institute of Medical Science, The University of Tokyo. The Animal Experiment Committee of the Institute of Medical Science, The University of Tokyo, approved all animal care and use in this study. A murine IL-3-dependent pro-B cell line, Ba/F3 [18], was cultured in RPMI 1640 medium (Nissui Pharmaceutical, Tokyo, Japan) supplemented with 10% fetal bovine serum (FBS) (Biowest, Paris, France) and 1 ng/ml murine IL-3 (R&D systems, Cambridge, MA). A human TF-1 cell line [19] was cultured in RPMI 1640 medium supplemented with 10% FBS, 10 mM HEPES and 2 ng/ml human granulocyte–macrophage colony-stimulating factor (GM-CSF) (R&D systems). A human T cell line Jurkat [20] was cultured in RPMI1640 medium supplemented with 10% FBS. Three retroviral packaging cell lines were used; Plat-E [21] was cultured in Dulbecco's modified Eagle's medium (DMEM) (Nissui Pharmaceutical) supplemented with 10% FBS, 1 μg/ml puromycin (Sigma, St Louis, MO) and 10 μg/ml blasticidin (Kaken Pharmaceutical, Tokyo, Japan); 293GP [22] was cultured in DMEM supplemented with 10% FBS, and 293GPG [23] was cultured in DMEM supplemented with 10% FBS, 2 μg/ml puromycin, 300 μg/ml G418 (Calbiochem, Darmstadt, Germany) and 1 μg/ml tetracycline (Sigma).

2.3. Purification of murine CD34⁻KSL HSCs

$CD34^{-/low}$c-$Kit^{+}Sca\text{-}1^{+}Lin^{-}$ ($CD34^{-}$KSL) HSCs were purified from bone marrow of C57BL/6-Ly5.1 mice, as previously described [24,25]. Briefly, bone marrow cells were stained with a lineage antibody mixture consisting of anti-Gr-1, Mac-1, B220, CD4, CD8 and Ter-119 monoclonal antibodies (BD Biosciences, Franklin Lakes, NJ), and magnetic beads-conjugated anti-rat IgG secondary antibody (Miltenyi, Auburn, CA), followed by depletion of lineage-positive cells using magnetic cell sorting. The cells were subsequently stained with phycoerythrin (PE)-conjugated anti-Sca-1, allophycocyanin (APC)-conjugated anti-c Kit, fluorescein isothiocyanate (FITC)-conjugated anti-CD34 and biotin-conjugated lineage antibodies (all from BD Biosciences) and APC-Cy7-conjugated streptavidin (Molecular Probes, Eugene, OR). $CD34^{-}$KSL HSCs were sorted into α-MEM containing 1% FBS, 100 ng/ml TPO and 100 ng/ml stem cell factor (SCF) (Peprotech, Rocky Hill, NJ) using a MoFlo Cell Sorter (Beckman Coulter, Fullerton, CA).

2.4. Vector transduction

Plat-E cells were transfected with pMK-S-Mpl-IG using Lipofectamine LTX (Invitrogen) according to the manufacturer's protocol, and the culture medium was used as a viral supernatant for transduction of Ba/F3 cells. Ba/F3 cells were transduced with the viral supernatant in the presence of 2 ng/ml IL-3 in a 24-well plate, using RetroNectin (TAKARA Bio, Shiga, Japan) according to the manufacturer's instructions, and the transduced cells were designated as Ba/S-Mpl.

For the transduction of mouse $CD34^{-}$KSL HSCs, a stable virus producer cell line based on 293GPG cells was established. A retroviral packaging cell line 293GP was co-transfected with the pGCDNsam expression vector and the pcDNA3.1-VSV-G vector encoding a VSV-G envelope gene by lipofection for a transient production of VSV-G pseudotyped retroviruses. The culture medium of the transfected 293GP was collected and subsequently used for transduction of 293GPG, which had been engineered to express the VSV-G protein under control of a tetracycline-inducible system [23]. 293GPG cells transduced with GCDNsam-S-Mpl-I/E or GCDNsam-I/E stably produced retroviruses encoding the respective genes. The culture supernatant of the transduced 293GPG was collected and centrifuged at 6000*g* for 16 h at 4 °C, followed by resuspension of the viral pellet in a StemPro-34 SFM (Invitrogen) to obtain a 100-fold concentrated virus. Virus titers were determined by infection of Jurkat cells based on the EGFP-positive cell ratio on day 2. $CD34^{-}$KSL HSCs cultured overnight after sorting were transduced with the virus at multiplicity of infection (MOI) of 500 in the presence of SCF and TPO (100 ng/ml each) in a 96-well plate, using RetroNectin. The transduced cells were designated as HSC/S-Mpl or HSC/mock, respectively.

2.5. Selection of the Ba/F3 transductants and cell proliferation assay

For selection of the Ba/F3 transductants, the cells were washed with PBS and inoculated into 24-well plates. Ba/S-Mpl was selected in the medium containing either no factor, 5 μg/ml BSA-FL or 1 ng/ml IL-3. For the cell proliferation assay, the selected cells were washed with PBS and were seeded into 24-well plates at 5×10^3 cells/ml with the indicated concentrations of each ligand. The viable cell numbers were counted using a FACS Calibur flow cytometer (Becton Dickinson, Lexington, KY).

2.6. Western blotting

The cells (10^6 cells) were washed with PBS, lysed with 100 μl of lysis buffer (20 mM HEPES, 150 mM NaCl, 10% glycerol, 1% Triton X-100, 1.5 mM $MgCl_2$, 1 mM EGTA, 10 μg/ml aprotinin, 10 μg/ml leupeptin, pH 7.5) and incubated on ice for 10 min. After centrifugation at 16,000*g* for 10 min, the supernatant was mixed with Laemmli's sample buffer and boiled. The lysate was resolved by SDS–PAGE and transferred to a nitrocellulose membrane (Millipore, Bedford, MA). After the membrane was blocked with 5% skimmed milk or 1% BSA, the blot was probed with appropriate dilutions of primary and secondary antibodies, and detection was performed using Chemi-Lumi One (Nacalai Tesque, Kyoto, Japan). The primary rabbit antibodies anti-mouse STAT3 and anti-mouse ERK1 were purchased from Santa Cruz Biotechnology (Santa Cruz, CA); anti-human c-Mpl was from Upstate Biotechnology (Lake Placid, NY); anti-phospho-ERK1 was from Promega (Madison, WI); anti-phospho-STAT3 was from Cell Signaling Technology (Danvers, MA), and HRP-conjugated anti-rabbit IgG was purchased from Biosource (Camarillo, CA).

2.7. Starvation and stimulation of cells

Cells were washed three times with PBS and starved in the depletion medium (RPMI 1640, 10% FBS) for 24 h. The cells (4.3×10^6) were stimulated with 4 ml medium containing no ligand, 1 ng/ml IL-3 or 5 μg/ml BSA-FL at 37 °C. After incubation for 15 min, the cells were exposed to 4 ml of 2 mM ice-cold Na_3VO_4 in PBS, pelleted and lysed with 100 μl/10^6 cells of lysis buffer to prepare lysates for Western blot analysis.

2.8. In vitro growth assay of HSCs

The medium of the transduced $CD34^-KSL$ HSCs was exchanged into S-clone SF-03 (Sanko Junyaku Inc., Tokyo, Japan) containing 50 ng/ml TPO and 50 ng/ml SCF on the day after transduction, and the cells were cultured for 2 days. The cells were washed with PBS containing 2% FBS and seeded into 96-well plates with either no factor, 50 ng/ml TPO, 50 ng/ml SCF, 5 μg/ml BSA-FL, 50 ng/ml TPO plus 50 ng/ml SCF, or 50 ng/ml SCF plus 5 μg/ml BSA-FL in the S-clone SF-03. After cell culture for 5 days, the cells were washed with PBS once, and then mixed with Flow-count (Beckman Coulter) to analyze the cell number using a FACS Calibur flow cytometer. The remainder of the cells was cytospun onto glass slides and subjected to May–Grüenwald Giemsa staining for morphological examination.

2.9. Competitive repopulation assay of HSCs in vivo

Competitive repopulation assays were performed with the Ly5 congenic mouse system [24]. Donor cells from C57BL/6-Ly5.1 mice were prepared as follows: $CD34^-KSL$ cells were simply cultured in vitro with 50 ng/ml SCF plus 50 ng/ml TPO for 9 days as a control (designated as 'no transduction'). Another $CD34^-KSL$ cells were transduced with GCDNsam-S-Mpl-I/E vector on day 2. After 2-day culture, one portion of the transduced cells was transplanted into recipient mice (designated as 'no induction'). Another portion of the transduced cells was further cultured in vitro with either 50 ng/ml SCF, 50 ng/ml SCF plus 50 ng/ml TPO, or 50 ng/ml SCF plus 5 μg/ml BSA-FL for 5 days (designated as 'SCF', 'SCF + TPO', or 'SCF + BSA-FL', respectively). The expansion equivalent of ~40 purified HSCs, of which the number corresponds to the $CD34^-KSL$ cell number on day 0, was transplanted into each C57BL/6-Ly5.2 mouse irradiated at a dose of 4.75 Gy with 6.6×10^5 competitor cells from the bone marrow of C57BL/6-Ly5.1/5.2 F1 mice. Four and twelve weeks after transplantation, peripheral blood cells of the recipients were stained with PE-conjugated anti-Ly5.2, biotinylated anti-Ly5.1, PE-Cy7-conjugated anti-B220 and a mixture of APC-conjugated anti-CD4 and anti-CD8 antibodies (BD Biosciences). The biotinylated antibody was detected with streptavidin-Alexa594. The cells were analyzed on a FACS Vantage (Becton Dickinson). The percentage chimerism was calculated as (percentage Ly5.1−donor cells) × 100/(percentage Ly5.1−donor cells + percentage F1−competitor cells).

3. Results

3.1. Selective expansion of genetically modified Ba/F3 cells by BSA-FL

We designed an anti-fluorescein ScFv/c-Mpl chimera (S-Mpl) that can mimic a TPO-mediated growth signal in genetically modified cells (Fig. 1). We constructed the retroviral vector pMK-S-Mpl-IG, which allows expression of the EGFP marker gene together with the S-Mpl gene, thus enabling identification of genetically modified cells. Previous reports have described that ectopic expression of c-Mpl in an IL-3-dependent murine pro-B cell line Ba/F3 was sufficient for cell proliferation in response to the cognate ligand, TPO [26,27]. Thus, we first performed a functional analysis of S-Mpl chimera using Ba/F3 cells.

Ba/F3 cells were transduced with MK-S-Mpl-IG retroviral vector to create Ba/S-Mpl cells. For selection of the transductant, we used BSA-FL as a ligand, because multiple fluorescein molecules in BSA-FL would facilitate oligomerization of the chimera and trigger a growth signal. The Ba/F3 transductant was selected in the media with no ligand, 5 μg/ml BSA-FL or 1 ng/ml IL-3 for 15 days, followed by a flow cytometric analysis to examine EGFP-positive cell ratios. Consequently, while the cells cultured with no ligand were

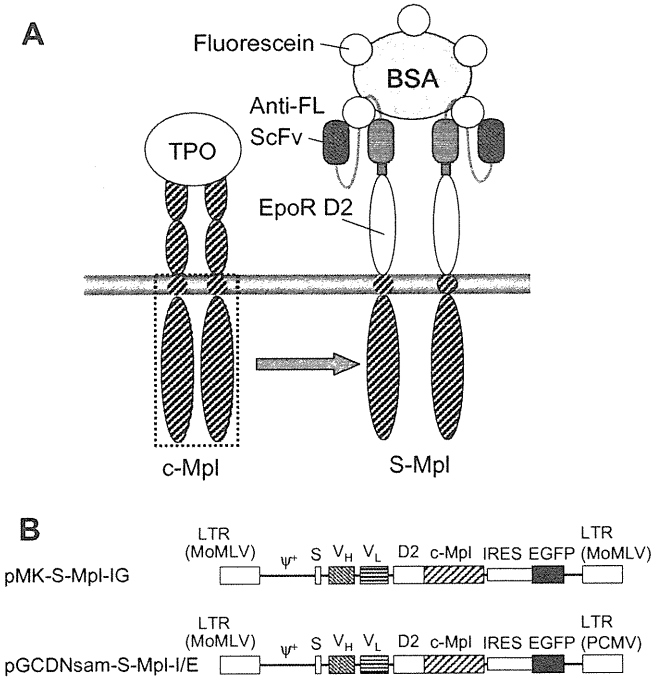

Fig. 1. The constructs of the chimeric receptor, S-Mpl. (A) A schematic illustration of wild-type and chimeric c-Mpl. In the S-Mpl chimera, a single-chain Fv (ScFv) of an anti-fluorescein antibody was tethered to the extracellular D2 domain of the erythropoietin receptor and transmembrane/cytoplasmic domains of c-Mpl. (B) The construction of the chimeric c-Mpl vectors. The pMK retroviral vector had a 5' Moloney murine leukemia virus (MoMLV) long terminal repeat (LTR), 3' MoMLV LTR and a packaging signal (Ψ). The pGCDNsam retroviral vector had a 5' MoMLV LTR, 3' PCC4 cell-passaged myeloproliferative sarcoma virus (PCMV) LTR and a packaging signal (Ψ^+). An immunoglobulin heavy chain secretion signal sequence (S) was placed upstream of the chimeric receptor gene for cell surface expression.

unable to grow, the cells cultured with BSA-FL showed vigorous proliferation. The EGFP-positive cell ratio of the BSA-FL-selected cells was almost 100%, while those of the IL-3-selected cells were less than those before selection (Fig. 2A).

To investigate whether cell proliferation during BSA-FL selection was induced by the expressed S-Mpl chimera, the expression of the chimera was confirmed by Western blotting. BSA-FL-selected transductants exclusively showed a distinct band of S-Mpl migrating around 54 kD (Fig. 2B). These results indicate that only the cells expressing the S-Mpl chimera can grow in response to BSA-FL, leading to selective expansion of the genetically modified Ba/F3 cells.

3.2. BSA-FL dependent cell proliferation and activation of signal transducers

We next performed a cell proliferation assay to evaluate whether the growth of the BSA-FL-selected Ba/S-Mpl cells is promoted in a BSA-FL dose-dependent manner. Indeed, when the Ba/S-Mpl cells were cultured in the media containing various concentrations of BSA-FL, the cells showed BSA-FL dose-dependent cell proliferation (Fig. 3A). The lower limit for BSA-FL-dependent cell growth was between 0.01 and 0.1 μg/ml, while the BSA-FL concentration below 0.01 μg/ml did not induce any cell growth during the culture period tested. Therefore, S-Mpl chimera could promote the proliferation of the genetically modified cells in a BSA-FL-dependent manner without any apparent background cell growth.

Homodimerization of c-Mpl triggers downstream signaling events that involve the phosphorylation of various cellular proteins. The c-Mpl signaling mainly activates Jak/STAT and Ras/MAPK pathways through cellular protein kinases [28–30]. Activated JAK2 or TYK2 is able to phosphorylate signal transducers and activator of transcription (STATs) 1, 3 and 5. The phosphorylation of STAT molecules induces their dimerization, resulting in their translocation to the nucleus, where they regulate gene transcriptions. The TPO binding also induces tyrosine phosphorylation of c-Mpl, resulting in the recruitment of Shc and Grb2, followed by the activation of the Ras/MAPK pathway. To examine whether the S-Mpl chimera could mimic c-Mpl-mediated signaling, the phosphorylation status of STAT3 and ERK1 was examined by Western blotting (Fig. 3B). When Ba/S-Mpl was stimulated with BSA-FL, both ERK1 and STAT3 were phosphorylated, while the phosphorylation of these signal transducers was not detected in the parental Ba/F3 cells stimulated with BSA-FL. Although weak activation of ERK1 and STAT3 was detected in the Ba/S-Mpl cells without ligand stimulation, the hyperactivation was not strong enough for Ba/S-Mpl to grow without any ligand. Therefore, the S-Mpl chimera can successfully control

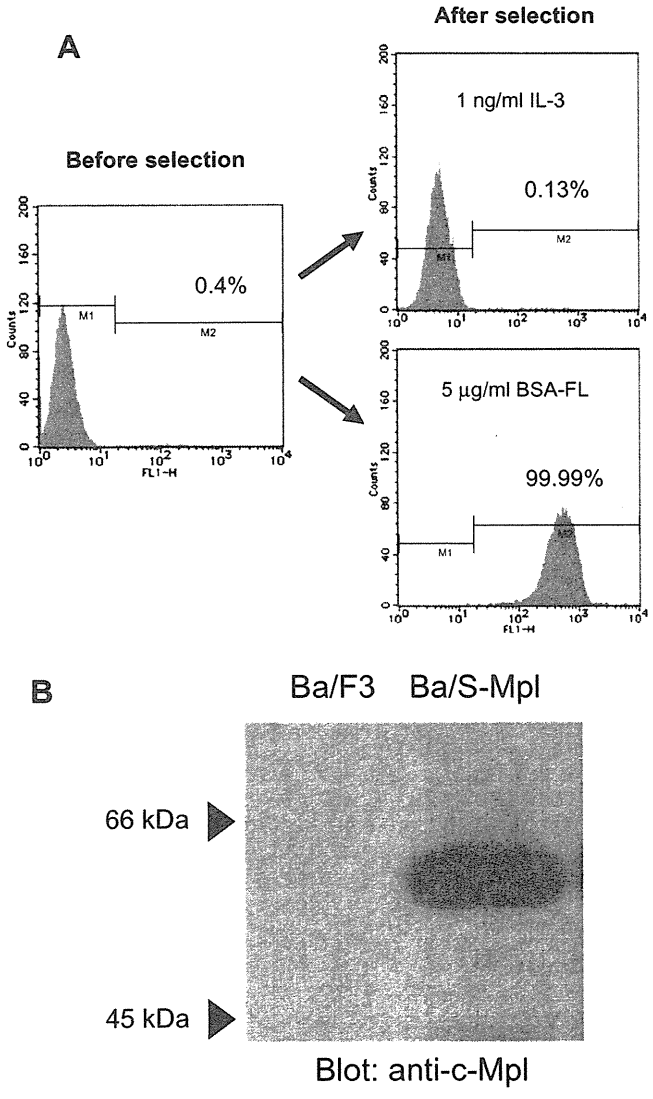

Fig. 2. Selective expansion of EGFP-positive cells with the S-Mpl chimera. (A) Ba/S-Mpl cells before and after selection (15 days) with 1 ng/ml IL-3 or 5 μg/ml BSA-FL were analyzed by flow cytometry. The cell number was plotted against the log green fluorescence intensity. EGFP-negative and EGFP-positive regions were determined by taking parental Ba/F3 cells as a negative control. The EGFP-positive cell ratios are indicated in each panel. (B) Western blot analysis to confirm the expression of the S-Mpl chimera in the BSA-FL-selected Ba/S-Mpl cells. The expression of the S-Mpl chimera was detected with an anti-c-Mpl antibody.

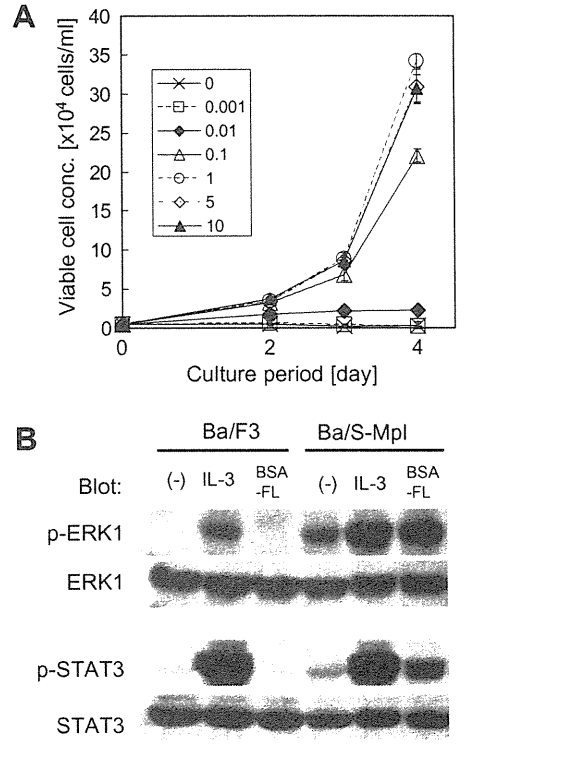

Fig. 3. BSA-FL-dependent cell growth and activation of signaling molecules in the Ba/S-Mpl cells. (A) BSA-FL-selected Ba/S-Mpl cells were inoculated into 24-well plates at day 0 (5×10^3 cells/ml) and cultured with the indicated concentrations of BSA-FL. The viable cell concentrations in triplicates are plotted as the average ± 1 SD. (B) Signal transduction to ERK1 and STAT3. Ba/F3 and Ba/S-Mpl cells were stimulated for 15 min with or without ligand (1 ng/ml IL-3 and 5 μg/ml BSA-FL). Western blot analysis was performed with anti-phospho-ERK1 and anti-phospho STAT3 antibodies to detect the phosphorylated form of each molecule, and with anti-ERK1 and anti-STAT3 antibodies to detect the whole molecules.

the proliferation of Ba/F3 cells through transducing a c-Mpl-like growth signal in response to the specific antigen.

3.3. In vitro culture of mouse HSCs expressing the S-Mpl chimera

We next investigated whether the S-Mpl chimera could be functional in HSCs (Fig. 4). Mouse HSCs were purified by flow cytometric sorting of $CD34^{-/low}c\text{-}Kit^{+}Sca\text{-}1^{+}Lin^{-}$ ($CD34^{-}KSL$) cells derived from the bone marrow of C57BL/6-Ly5.1 mice. To obtain high titers of retroviruses capable of transducing $CD34^{-}KSL$ cells with high efficiency, VSV-G pseudotyped retroviruses were prepared. The retroviral packaging cell line 293GPG was transduced with GCDNsam-S-Mpl-I/E, resulting in stable virus-producing cell lines named GPG/S-Mpl-IG. The culture supernatant of GPG/S-Mpl-IG was 100-fold concentrated by centrifugation and used for transduction of $CD34^{-}KSL$ cells. $CD34^{-}KSL$ cells were also transduced with mock vectors encoding an IG gene alone as a negative control.

Three days after transduction, the cells were cultured in the medium with no ligand, TPO alone, SCF alone, BSA-FL alone, SCF + TPO or SCF + BSA-FL. After a 5-day culture, viable cell numbers were measured using flow cytometry (Fig. 5A). Both mock-transduced and S-Mpl-transduced $CD34^{-}KSL$ cells cultured with no ligand or BSA-FL alone induced almost no growth, and those cultured with TPO alone or SCF alone induced some cell growth. In contrast, in S-Mpl-transduced $CD34^{-}KSL$ cells, the viable cell number was increased about 4-fold with SCF + BSA-FL compared to the cells cultured with SCF alone. Such an increase was not observed in the mock-transduced $CD34^{-}KSL$ cells. The culture with SCF + TPO led to a more than 3-fold increase of cell proliferation than that with SCF + BSA-FL, indicating that S-Mpl transduced a growth signal less efficiently than the wild-type c-Mpl. These data indicate that the S-Mpl chimera can transduce a growth signal in $CD34^{-}KSL$ cells.

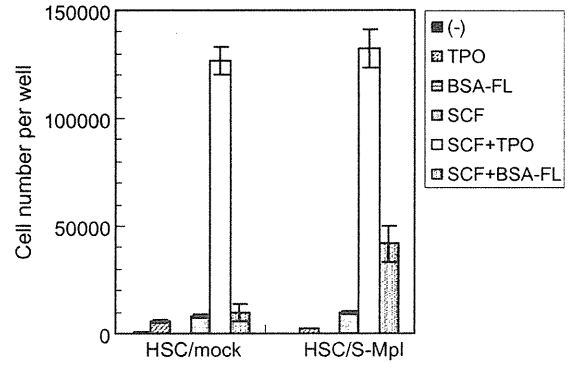

Fig. 5. In vitro growth assay of HSCs. The cells transduced with either GCDNsam-I/E control vector (HSC/mock) or GCDNsam-S-Mpl-I/E (HSC/S-Mpl) were washed and seeded into 96-well plates to test their proliferative responses in the indicated conditions. Each well received the expansion equivalent of ~40 fresh $CD34^{-}KSL$ cells. After cell culture for 5 days, the cells were mixed with Flow-count™ beads (Beckman Coulter) and enumerated using a FACS Calibur flow cytometer. Estimated cell numbers in triplicate cultures are plotted as the average ± 1 SD. (-): no ligand.

3.4. HSCs expressing the S-Mpl chimera can differentiate into multiple lineages in vivo

To investigate whether the S-Mpl-transduced $CD34^{-}KSL$ cells cultured with SCF + BSA-FL could function as HSCs in vivo, a competitive repopulation assay was performed. The S-Mpl-transduced $CD34^{-}KSL$ cells ($Ly5.1^{+}$) cultured with SCF alone, SCF + BSA-FL or SCF + TPO for 5 days were transplanted into irradiated mice ($Ly5.2^{+}$) together with bone marrow cells of a competitor mouse ($Ly5.1^{+}Ly5.2^{+}$). After 4 and 12 weeks, when we could detect early and long-term repopulating cells, respectively, peripheral blood cells were harvested to determine chimerism, namely, the Ly5.1

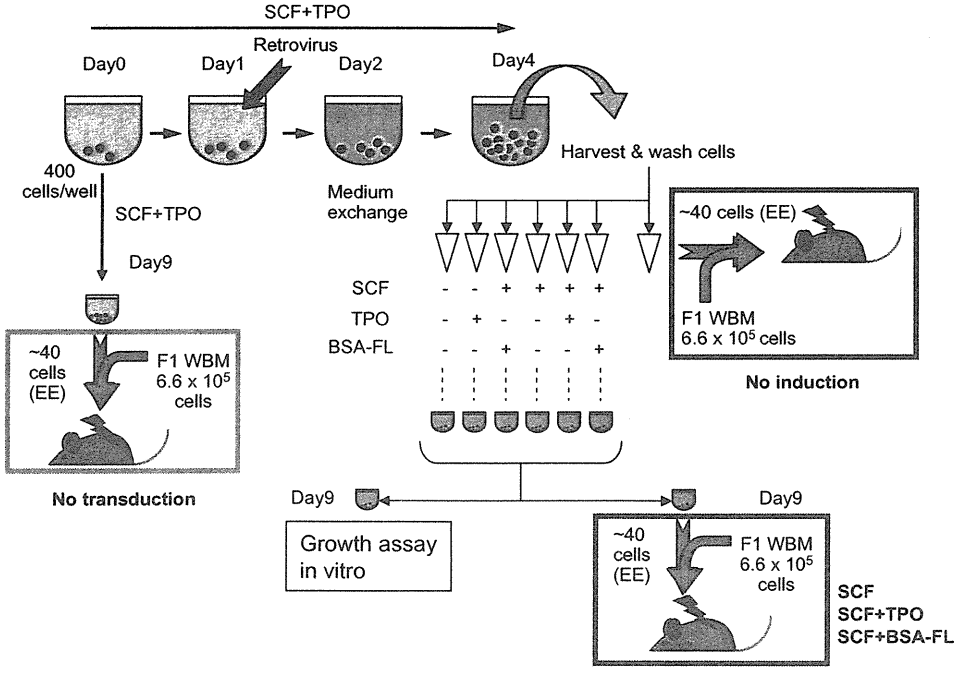

Fig. 4. Scheme of the HSC assays performed in vitro and in vivo. $CD34^{-}KSL$ cells of B6-Ly5.1 origin were sorted into a 96-well plate at 400 cells/well on day 0 and prestimulated with SCF + TPO, followed by retroviral transduction through days 1 and 2. Two days later (day 4), the cells were harvested and washed to remove the cytokines, and divided into culture wells to test their proliferative responses either in the absence of ligand or in the presence of varying combinations of SCF, TPO and BSA-FL as indicated. On day 9, the cell number was counted to compare the level of cellular expansion induced by each ligand combination. Marrow reconstitution ability was also tested in ex vivo cultured cells in a competitive repopulation assay: test cells (the expansion equivalent (EE) of ~40 fresh $CD34^{-}KSL$ cells) were transplanted into each lethally irradiated recipient mouse (Ly5.2) together with 6.6×10^5 whole bone marrow (WBM) competitor cells prepared from Ly5.1/Ly5.2 F1 mice. The cells cultured for 9 days with SCF + TPO but with no retroviral transduction ('no transduction') and those transduced but harvested on day 4 without further cultivation ('no induction') were utilized as controls.

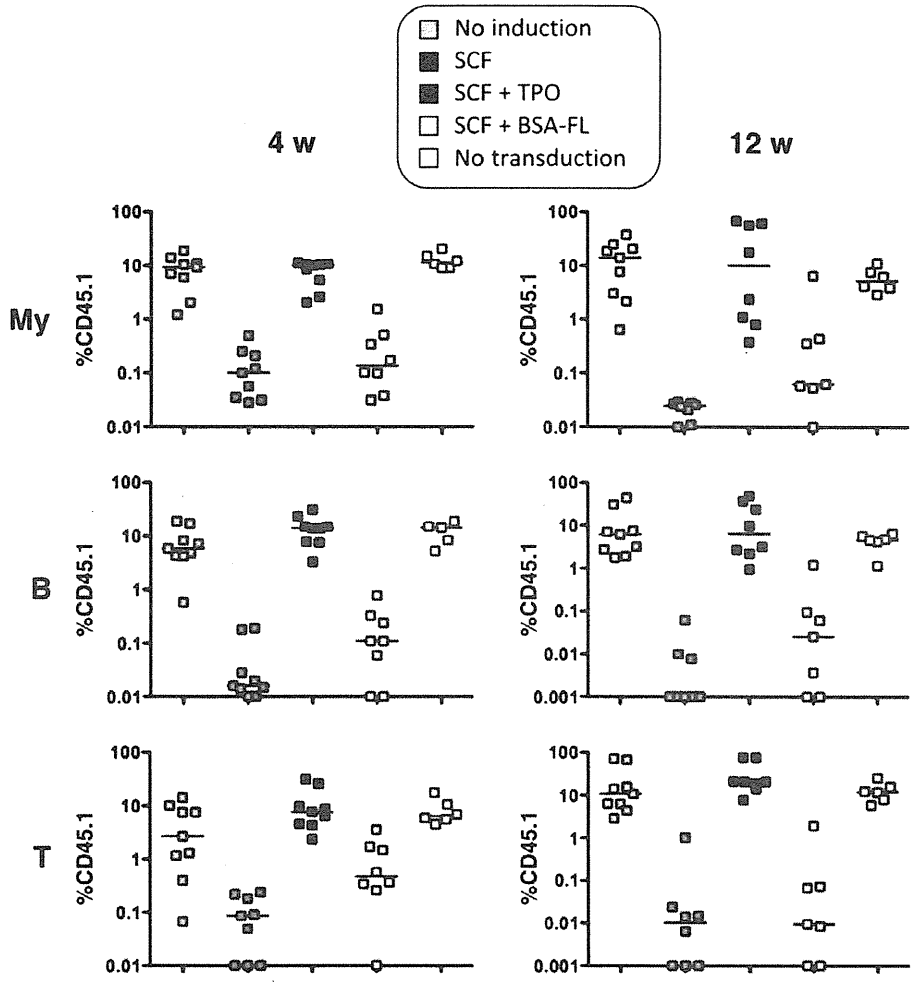

Fig. 6. Competitive repopulation assay to investigate the functionality of the ex vivo cultured HSCs. $CD34^-KSL$ cells transduced with GCDNsam-S-Mpl-I/E were cultured for another 5 days in the presence of either SCF, SCF + TPO or SCF + BSA-FL, and tested for their marrow reconstitution ability as detailed in Fig. 4. Shown are percent test cell chimerisms in donor cells [$\%CD45.1^+/(CD45.1^+ + CD45.1/45.2$ F1) cells] assessed in the peripheral blood of recipients after 4 weeks (4 w) and 12 weeks (12 w) after transplantation. Values obtained with 'no transduction' and 'no induction' control cells are also shown. Chimerism was analyzed separately on myeloid lineage cells (My), T lymphocytes (T) and B lymphocytes (B) by gating on their markers. The median values are indicated as bars.

single-positive cell ratio, in myeloid, T and B cells. As a result, there was a tendency that the chimerism values in SCF + BSA-FL were retained higher than those in SCF alone for all lineages and time points (Fig. 6), which correlates the results of the growth assay in vitro. Notably, the chimerism values remained almost constant from 4 to 12 weeks, indicating that the S-Mpl-transduced $CD34^-KSL$ cells can retain long-term multi-lineage repopulation ability in vivo.

4. Discussion

In this study, we first showed that the S-Mpl chimera is functional in Ba/F3 cells. In our previous studies, Ba/F3 cells expressing either S-gp130, S-EpoR, S-IL-2R, S-EGFR or S-Fms showed cell growth in response to BSA-FL. Although S-IL-2R chimera transduced a strictly BSA-FL-dependent growth signal [10], considerable background growth was observed for other chimeras [7–9,11]. In S-gp130 and S-EpoR chimeras, we constructed a series of chimeras whose extracellular domain contained either D1 domain, D2 domain, D1 and D2 domain, or nothing, and whose rotational angle of the intracellular domain was modulated by alanine insertion. While we successfully found out a strictly BSA-FL-dependent derivative for the S-gp130 chimera using such an approach [9], the signals through all the S-EpoR derivatives were not tightly controllable by BSA-FL [8]. Thus, it is surprising that the growth signal through the S-Mpl chimera in this study was strictly dependent on BSA-FL. This might be owing to the property of c-Mpl itself, because Staerk et al. reported that an amphipathic motif (KWQFP) at the transmembrane-cytoplasmic junction could play an important role to prevent autonomous activation of c-Mpl [31]. The vigorous cell growth and activation of Mpl-mediated signal transducers in the presence of BSA-FL demonstrate that the S-Mpl chimera substantially mimicked wild-type c-Mpl signaling.

As for target cell types, this study is the first demonstration of an antibody/receptor chimera applied in highly purified HSCs. The viable cell number of S-Mpl-transduced $CD34^-KSL$ cells was increased ~4-fold with SCF + BSA-FL compared to the cells cultured with SCF alone. Furthermore, the competitive repopulation assay showed the long-term existence of both myeloid and lymphoid cells derived from the test HSCs, demonstrating that S-Mpl-transduced HSCs cultured in SCF + BSA-FL were able to retain functional HSCs. The culture in SCF + BSA-FL resulted in significantly higher test cell chimerism especially in the myeloid lineage than the culture in SCF alone, indicating that HSCs retaining reconstitution capability were better maintained with the culture in BSA-FL-mediated S-Mpl signaling. Collectively, it was demonstrated that the S-Mpl chimera functionally mimicked wild-type

c-Mpl. A remaining concern of the S-Mpl chimera may be the magnitude of the cellular expansion level driven by this molecule, which was significantly less than that mediated by endogenous wild-type c-Mpl. This issue may be solved by further molecular modification of the S-Mpl chimera that will maximize the signal transduction efficiency.

Until now, other molecular switches to expand genetically modified cells have been reported. Gyrase B, an estrogen receptor mutant and an FK506-binding protein 12 (FKBP12) mutant were used as ligand-binding domains and fused to the intracellular domain of cytokine receptors. These fusion proteins led to successful cellular expansion in response to coumermycin, 4-hydroxytamoxifen and AP20187 (or its derivatives called chemical inducers of dimerization), respectively [32–34]. Although these methods can be used for the expansion of a single transduced cell population, the expansion of multiple cell populations transduced by different transgenes cannot be individually controlled by respective specific ligands. Since the number of antigen–antibody pairs is almost infinite, various antibody/receptor chimeras responsive to different antigens could realize controlling the fate of a wide variety of cell populations, and provide new directions for stem cell-based therapies.

Acknowledgments

We are grateful to Dr. T. Kitamura (The University of Tokyo) for the pMX-based retroviral expression system, and Dr. I.M. Tomlinson (Domantis, Cambridge, UK) for the anti-FL antibody ScFv. This work was supported by Grants-in-Aid for Scientific Research (A) 18206083 (T.N.) and for Young Scientists (A) 21686077 (M.K.) from the MEXT, Japan, by the Program for Promotion of Basic and Applied Researches for Innovations in Bio-oriented Industry (BRAIN) and by the Global COE Program for Chemistry Innovation.

References

[1] Livnah O, Stura EA, Middleton SA, Johnson DL, Jolliffe LK, Wilson IA. Crystallographic evidence for preformed dimers of erythropoietin receptor before ligand activation. Science 1999;283:987–90.
[2] Damjanovich S, Bene L, Matko J, Alileche A, Goldman CK, Sharrow S, et al. Preassembly of interleukin 2 (IL-2) receptor subunits on resting Kit 225 K6 T cells and their modulation by IL-2, IL-7, and IL-15: a fluorescence resonance energy transfer study. Proc Natl Acad Sci USA 1997;94:13134–9.
[3] Giese B, Roderburg C, Sommerauer M, Wortmann SB, Metz S, Heinrich PC, et al. Dimerization of the cytokine receptors gp130 and LIFR analysed in single cells. J Cell Sci 2005;118:5129–40.
[4] Tenhumberg S, Schuster B, Zhu L, Kovaleva M, Scheller J, Kallen KJ, et al. gp130 dimerization in the absence of ligand: preformed cytokine receptor complexes. Biochem Biophys Res Commun 2006;346:649–57.
[5] Remy I, Wilson IA, Michnick SW. Erythropoietin receptor activation by a ligand-induced conformation change. Science 1999;283:990–3.
[6] Blakely BT, Rossi FM, Tillotson B, Palmer M, Estelles A, Blau HM. Epidermal growth factor receptor dimerization monitored in live cells. Nat Biotechnol 2000;18:218–22.
[7] Kawahara M, Kimura H, Ueda H, Nagamune T. Selection of genetically modified cell population using hapten-specific antibody/receptor chimera. Biochem Biophys Res Commun 2004;315:132–8.
[8] Liu W, Kawahara M, Ueda H, Nagamune T. The influence of domain structures on the signal transduction of chimeric receptors derived from the erythropoietin receptor. J Biochem 2009;145:575–84.
[9] Liu W, Kawahara M, Ueda H, Nagamune T. Construction of a fluorescein-responsive chimeric receptor with strict ligand dependency. Biotechnol Bioeng 2008;101:975–84.
[10] Sogo T, Kawahara M, Ueda H, Otsu M, Onodera M, Nakauchi H, et al. T cell growth control using hapten-specific antibody/interleukin-2 receptor chimera. Cytokine 2009;46:127–36.
[11] Tanaka K, Kawahara M, Ueda H, Nagamune T. Selection and growth regulation of genetically modified cells with hapten-specific antibody/receptor tyrosine kinase chimera. Biotechnol Prog 2009;25:1138–45.
[12] Pihkala P, Kawahara M, Ueda H, Nagamune T. An antigen-mediated selection system for mammalian cells that produce glycosylated single-chain Fv. Biochem Biophys Res Commun 2004;324:1165–72.
[13] Kawahara M, Ogo Y, Ueda H, Nagamune T. Improved growth response of antibody/receptor chimera attained by the engineering of transmembrane domain. Protein Eng Des Sel 2004;17:715–9.
[14] Yagi M, Ritchie KA, Sitnicka E, Storey C, Roth GJ, Bartelmez S. Sustained ex vivo expansion of hematopoietic stem cells mediated by thrombopoietin. Proc Natl Acad Sci USA 1999;96:8126–31.
[15] Suzuki A, Obi K, Urabe T, Hayakawa H, Yamada M, Kaneko S, et al. Feasibility of ex vivo gene therapy for neurological disorders using the new retroviral vector GCDNsap packaged in the vesicular stomatitis virus G protein. J Neurochem 2002;82:953–60.
[16] Nabekura T, Otsu M, Nagasawa T, Nakauchi H, Onodera M. Potent vaccine therapy with dendritic cells genetically modified by the gene-silencing-resistant retroviral vector GCDNsap. Mol Ther 2006;13:301–9.
[17] Sanuki S, Hamanaka S, Kaneko S, Otsu M, Karasawa S, Miyawaki A, et al. A new red fluorescent protein that allows efficient marking of murine hematopoietic stem cells. J Gene Med 2008;10:965–71.
[18] Palacios R, Steinmetz M. IL-3-dependent mouse clones that express B-220 surface antigen, contain Ig genes in germ-line configuration, and generate B lymphocytes in vivo. Cell 1985;41:727–34.
[19] Kitamura T, Tange T, Terasawa T, Chiba S, Kuwaki T, Miyagawa K, et al. Establishment and characterization of a unique human cell line that proliferates dependently on GM-CSF, IL-3, or erythropoietin. J Cell Physiol 1989;140:323–34.
[20] Schneider U, Schwenk HU, Bornkamm G. Characterization of EBV-genome negative "null" and "T" cell lines derived from children with acute lymphoblastic leukemia and leukemic transformed non-Hodgkin lymphoma. Int J Cancer 1977;19:621–6.
[21] Morita S, Kojima T, Kitamura T. Plat-E: an efficient and stable system for transient packaging of retroviruses. Gene Ther 2000;7:1063–6.
[22] Burns JC, Friedmann T, Driever W, Burrascano M, Yee JK. Vesicular stomatitis virus G glycoprotein pseudotyped retroviral vectors: concentration to very high titer and efficient gene transfer into mammalian and nonmammalian cells. Proc Natl Acad Sci USA 1993;90:8033–7.
[23] Ory DS, Neugeboren BA, Mulligan RC. A stable human-derived packaging cell line for production of high titer retrovirus/vesicular stomatitis virus G pseudotypes. Proc Natl Acad Sci USA 1996;93:11400–6.
[24] Ema H, Takano H, Sudo K, Nakauchi H. In vitro self-renewal division of hematopoietic stem cells. J Exp Med 2000;192:1281–8.
[25] Osawa M, Hanada K, Hamada H, Nakauchi H. Long-term lymphohematopoietic reconstitution by a single CD34-low/negative hematopoietic stem cell. Science 1996;273:242–5.
[26] Lok S, Kaushansky K, Holly RD, Kuijper JL, Lofton-Day CE, Oort PJ, et al. Cloning and expression of murine thrombopoietin cDNA and stimulation of platelet production in vivo. Nature 1994;369:565–8.
[27] Park H, Hong HJ. Development of an in vitro bioassay system for human thrombopoietin by constructing a recombinant murine cell line expressing human thrombopoietin receptor. Mol Cells 1997;7:699–704.
[28] Kaushansky K. The molecular mechanisms that control thrombopoiesis. J Clin Invest 2005;115:3339–47.
[29] Matsumura I, Nakajima K, Wakao H, Hattori S, Hashimoto K, Sugahara H, et al. Involvement of prolonged RAS activation in thrombopoietin-induced megakaryocytic differentiation of a human factor-dependent hematopoietic cell line. Mol Cell Biol 1998;18:4282–90.
[30] Takatoku M, Kametaka M, Shimizu R, Miura Y, Komatsu N. Identification of functional domains of the human thrombopoietin receptor required for growth and differentiation of megakaryocytic cells. J Biol Chem 1997;272:7259–63.
[31] Staerk J, Lacout C, Sato T, Smith SO, Vainchenker W, Constantinescu SN. An amphipathic motif at the transmembrane-cytoplasmic junction prevents autonomous activation of the thrombopoietin receptor. Blood 2006;107:1864–71.
[32] Kume A, Ito K, Ueda Y, Hasegawa M, Urabe M, Mano H, et al. A G-CSF receptor-gyrase B fusion gene: A new type of molecular switch for expansion of genetically modified hematopoietic cells. Biochem Biophys Res Commun 1999;260:9–12.
[33] Xu R, Kume A, Matsuda KM, Ueda Y, Kodaira H, Ogasawara Y, et al. A selective amplifier gene for tamoxifen-inducible expansion of hematopoietic cells. J Gene Med 1999;1:236–44.
[34] Jin L, Zeng H, Chien S, Otto KG, Richard RE, Emery DW, et al. In vivo selection using a cell-growth switch. Nat Genet 2000;26:64–6.

Intracellular estrogen receptor-binding fragment-associated antigen 9 exerts *in vivo* tumor-promoting effects via its coiled-coil region

YOSHIHIRO MAEYAMA[1,2], MAKOTO OTSU[3], SHUJI KUBO[4], TOMOKI YAMANO[5], YASUAKI IIMURA[1,2], MASAFUMI ONODERA[6], SATOSHI KONDO[2], YUKIO SAKIYAMA[1] and TADASHI ARIGA[1,7]

[1]Group of Human Gene Therapy, [2]Department of Surgical Oncology, Hokkaido University Graduate School of Medicine, N15W7 Sapporo, Hokkaido 060-8638; [3]Division of Stem Cell Therapy, Center for Stem Cell Biology and Regenerative Medicine, The Institute of Medical Science, The University of Tokyo, 4-6-1 Shirokanedai, Minato-ku, Tokyo 108-8639; [4]Department of Genetics and [5]Division of Lower Gastrointestinal Surgery, Department of Surgery, Hyogo College of Medicine, 1-1 Mukogawa-cho, Nishinomiya, Hyogo 663-8501; [6]Department of Human Genetics, National Center for Child Health and Development, 2-10-1 Okura, Setagaya-ku, Tokyo 157-8535; [7]Department of Pediatrics, Hokkaido University Graduate School of Medicine, N15W7 Sapporo, Hokkaido 060-8638, Japan

Received February 22, 2011; Accepted April 6, 2011

DOI: 10.3892/ijo.2011.1026

Abstract. Estrogen receptor-binding fragment-associated antigen 9 (EBAG9) is a tumor-promoting factor of largely unknown function. To assess a causative role of EBAG9 in advanced malignancies, we generated the EG7-OVA and MethA murine tumor cell lines that stably express full-length or truncated EBAG9 protein, using retroviral-mediated gene transduction. Upon subcutaneous inoculation into immunocompetent mice, both cell lines showed marked acceleration of *in vivo* tumor growth when full-length EBAG9 was overexpressed. Interestingly, deletion of the coiled-coil region, thereby producing truncated EBAG9 protein, abolished the tumor-acceleration effect, establishing the importance of this domain in EBAG9-mediated tumor promotion. However, there was no alteration in *in vitro* cell proliferation or expression levels of MHC class I and co-stimulatory molecules believed to play a role in immune evasion of tumor cells in these tumor cell lines expressing full-length or truncated EBAG9 protein. Furthermore, both full-length and truncated EBAG9 proteins showed a predominantly cytoplasmic localization in the tumor cells. Collectively, these results suggest that EBAG9 overexpression can be causative in enhancing the malignant properties of tumor cells, and that tumor promotion likely requires EBAG9 intracellular association with as yet unidentified binding partners via the coiled-coil region.

Correspondence to: Dr Tadashi Ariga, Department of Pediatrics, Hokkaido University Graduate School of Medicine, N15W7 Sapporo, Hokkaido 060-8638, Japan
E-mail: tada-ari@med.hokudai.ac.jp

Dr Shuji Kubo, Department of Genetics, Hyogo College of Medicine, 1-1 Mukogawa-cho, Nishinomiya, Hyogo 663-8501, Japan
E-mail: s-kubo@hyo-med.ac.jp

Key words: estrogen receptor-binding fragment-associated antigen 9, tumor promotion, coiled-coil region

Introduction

Identification of the molecules responsible for the development and/or progression of certain malignant tumors has marked significant progress in clinical cancer research, as such molecules serve as prognostic markers and/or therapeutic targets. Recently, estrogen receptor-binding fragment-associated antigen 9 (EBAG9) has come under scrutiny (1). EBAG9 is a ubiquitously expressed protein encoded by an estrogen-responsive gene (1). Studies have suggested that EBAG9 is linked to advanced malignancies, although its function remains undetermined (2-5). Nakashima *et al* (6) demonstrated that EBAG9 was a type II membrane protein that had a C-terminal coiled-coil region at the cell surface that could bind to the putative receptor in T cells and NK cells, thereby inducing their apoptotic cell death (6), and named it receptor-binding cancer antigen expressed on SiSo cells (RCAS1). However, Engelsberg *et al* presented a new finding that EBAG9 was a Golgi-resident protein that modulates cell surface glycosylation by a series of biochemical and cellular imaging analyses (7-11). They proposed that EBAG9-overexpression might contribute to the antigenicity of tumor cells by generation of the tumor-associated *O*-linked glycan Tn antigen (for example, 22.1.1 antigen).

Recently, Ogushi *et al* demonstrated that the overexpression of EBAG9 in a murine renal carcinoma cell line enhanced *in vivo* tumorigenesis, providing the first evidence of a tumor-promoting function for EBAG9 (12). They also suggested the

involvement of an immune-evasion mechanism in the observed effect mediated by EBAG9, but did not describe whether this overexpressed EBAG9 protein was localized on the cell surface or at the Golgi membrane to exert tumor promotion (12).

In the present study, we examined whether overexpression of EBAG9 would promote *in vivo* tumorigenesis in different syngeneic murine tumor models; EG7-OVA (EG7) tumor cells (13) in C57BL/6 mice and MethA cells (14) in BALB/c mice. Here we demonstrated that both cell lines engineered to express full-length EBAG9 protein showed marked acceleration of *in vivo* tumor growth on an immunocompetent background, without alteration in *in vitro* cell proliferation nor induction of the 22.1.1 antigen, which is thought to represent altered cell surface glycosylation induced by EBAG9-overexpression. Of note, deletion of the C-terminal coiled-coil region abolished tumor-promoting effects without altering its subcellular localization. Our data indicate that EBAG9-overexpression plays a causative role in advanced malignancies in an immunocompetent background, and also demonstrate the possibility that the cytoplasmic localization of EBAG9 with an intact C-terminal coding coiled-coil region is a prerequisite for the execution of *in vivo* tumor promotion.

Materials and methods

Cells. EG7 cells are C57BL/6 mouse lymphoma EL4 cell line transfected with ovalbumin (OVA) (13). MethA is a 3-methylcholanthrene-induced fibrosarcoma cell line of BALB/c mouse origin (14). These cell lines and Jurkat human T-cell leukemia cells were maintained in RPMI-1640 (Sigma, St. Louis, MO, USA) with 10% heat-inactivated fetal bovine serum (FBS; Moregate BioTech, Bulimba, Australia), 2 mM L-glutamine (Sigma), 100 U/ml penicillin-G (Sigma), and 100 μg/ml streptomycin (Sigma). The retrovirus packaging cell line, 293GP (15), was maintained in Dulbecco's modified Eagle's medium (DMEM) (Sigma) supplemented with 10% heat-inactivated FBS, 2 mM L-glutamine, 100 U/ml penicillin G, and 100 μg/ml streptomycin sulfate. Cells were cultured in a humidified 5% CO_2 at 37°C.

Construction and production of retroviral vectors. Full-length and truncated mouse EBAG9 cDNAs (EBAG9-FL and EBAG9-TR, respectively) were obtained by polymerase chain reaction (PCR) amplification using the first-strand DNA prepared from A20 mouse B lymphoma cells as templates. The truncated variants of EBAG9 cDNAs were designed to express EBAG9 protein lacking the C-terminal region (amino acids 179-213) encoding the coiled-coil region (Fig. 1A). The following primers were used for amplifying EBAG9-FL and EBAG9-TR cDNA: forward; 5'-CGTTTTCACCATGGCCAT CAC-3', reverse for full-length: 5'-CATAGCCTGTGTTAGGA AAGC-3', reverse for truncated: 5'-CTCAAATTTTCTGCT GCCTCAGCAC-3'.

These EBAG9 cDNAs were cloned into the transfer plasmid of the bicistronic retroviral vector expressing enhanced green fluorescent protein (EGFP) pGCDN IRES/EGFP (GCDN/EGFP for short), a derivative of the GCDNsap that was previously reported (16), generating retroviral vector transfer plasmids; pGCDN/EBAG9-FL and pGCDN/EBAG9-TR.

To produce vesicular stomatitis virus-G (VSV-G)-pseudotyped retroviral particles, packaging cell line 293GP was co-transfected with each transfer plasmid and pcDNA3.1-VSV-G, generating retroviral vector viruses; GCDN/EGFP, GCDN/EBAG9-FL and GCDN/EBAG9-TR. Vector supernatant was collected and subjected to subsequent concentration steps according to previously reported procedures (16).

Retroviral-mediated gene transduction of murine cell lines. EG7 and MethA cells were seeded at $1x10^5$ cells/well in 6-well plates and transduced by the addition of 50 μl of concentrated retroviral supernatant, followed by centrifugation at 2,000 rpm for 30 min at 32°C. Cells were cultured for 24 h at 37°C, and medium containing viral particles was replaced with fresh culture medium. Transduction efficiency was assessed 48-72 h later by determining the percentages of EGFP-positive cells using a FACSCalibur and the CellQuest software (Becton-Dickinson, San Jose, CA, USA). Transduction efficiencies commonly ranged between 20-80%. EG7 and MethA cells were sorted for an EGFP-positive population using a FACS Vantage Cell Sorter (Becton-Dickinson) (17).

Reverse transcription (RT)-PCR analysis. Total RNA samples were prepared from cells using the TRIzol reagent (Invitrogen, Carlsbad, CA, USA), followed by first-strand DNA synthesis using the SuperScript II kit (Invitrogen). Equal amounts of first-strand DNA were added to a mixture of 0.2 μM dNTP, 2.5 U Takara Taq DNA polymerase, 1X PCR buffer (Takara Bio, Otsu, Japan), and 0.4 μM each primer. The PCR consisted of 24 and 28 cycles (94°C for 30 sec 58°C for 30 sec, and 72°C for 30 sec), respectively, for amplification of EBAG9 and glyceraldehyde-3-phosphate dehydrogenase (GAPDH). The following primers were used for PCR amplification: EBAG9-forward (P1): 5'-TTGTACCTGCCTAGCAACAG-3', EBAG9-reverse (P2): 5'-AATTCAATGGTTCTCTCTTC-3', GAPDH-forward: 5'-TATTGGGCGCCTGGTCAC-3', GAPDH-reverse: 5'-AGATGATGACCCTTTTGGCTC-3'. The amplified products were separated on a 1.5% agarose gel and then visualized by UV light.

Cell proliferation assay. EG7 or MethA cells ($1x10^4$ cells/well) were seeded in 96-well flat-bottom plates and then cultured for 48 h. The extent of cell proliferation was assessed using the Cell Proliferation Kit I (Roche Diagnostics, Indianapolis, IN, USA), which utilizes 3-(4,5-dimethyl-2-thiazolyl)-2,5-dipenyl-2H-tetrazolium bromide (MTT) as an indicator of metabolic activity of viable cells, according to the manufacturer's instructions.

In vivo experiments. All procedures involving animals were approved by and performed according to guidelines of the Institutional Animal Care and Use Committee of Hokkaido University Graduate School of Medicine. Female C57BL/6 (H-2^b) and BALB/c (H-2^d) mice (5-8 week of age; CLEA Japan, Tokyo, Japan) were injected s.c. into the abdominal flank of unconditioned mice with $2.5x10^6$ tumor cells that was untransduced or transduced with vectors carrying EGFP, EBAG9-FL or EBAG9-TR (n=6 in each group). Tumors were measured three times per week, and tumor volumes were calculated as $a \times b^2 \times 0.5$ (a, large diameter; b, small diameter). The following